DOCTORAL DISSERTATION

博士論文

MODELING OF PARTICLE CRUSHING BASED ON GENERALIZED EVOLUTION LAW FOR GRADING

一般化された粒度の発展則に基づく粒子破砕現象のモデル化

FLORINCE

フローリンス

YOKOHAMA NATIONAL UNIVERSITY

Graduate School of Urban Innovation

国立大学法人横浜国立大学大学院都市イノベーション学府

March 2024

令和 6 年 3 月

MODELING OF PARTICLE CRUSHING BASED ON GENERALIZED EVOLUTION LAW FOR GRADING

(一般化された粒度の発展則に基づく粒子破砕現象のモデル化)

by

FLORINCE

フローリンス

A dissertation submitted to the Graduate School of Urban Innovation, Yokohama National University in partial fulfillment of the requirement for the Degree of

Doctor of Engineering

Graduate School of Urban Innovation

Yokohama National University

国立大学法人横浜国立大学大学院都市イノベーション学府

Examination Committee

Professor, Dr. Mamoru KIKUMOTO (Chair)

Professor, Dr. Kimitoshi HAYANO

Associate Professor, Dr. Ying CUI

Professor, Dr. Chikako FUJIYAMA

Associate Professor, Dr. Hiroshi TAMURA

March 2024

令和 6 年 3 月

ACKNOWLEDGMENT

I would like to express my deepest gratitude to everyone who has contributed to the completion of this dissertation. This journey has been filled with obstacles, yet it has also been an enlightening experience.

Above all, I express my profound gratitude to my Lord and Savior, Jesus Christ, who has been my guiding light, source of strength, and constant companion through all the seasons of my life.

I extend my sincere gratitude to my supervisor, Professor Mamoru Kikumoto, whose guidance and expertise have been invaluable throughout this research endeavor. Your insightful feedback and unwavering support have shaped not only the content of this dissertation but also my growth as a researcher. I am also grateful to the members of my dissertation committee, Professor Kimitoshi Hayano, Associate Professor Ying Cui, Professor Chikako Fujiyama, and Associate Professor Hiroshi Tamura, for the guidance during my study and for the constructive criticism and valuable input to improve the quality of this work.

I extend my heartfelt thanks to all mentors, colleagues, and classmates who have been a source of inspiration. The exchange of ideas and the shared experiences have played a crucial role in shaping the direction of my research.

I would like to acknowledge the financial support provided by Yokohama National University and the Ministry of Education, Culture and Sports, Science and Technology, Japan for providing me great opportunity and financial support to fulfill my PhD degree.

Last but not least, to my friends and family in Japan and Indonesia, thank you for your love and encouragement during the highs and lows of this academic journey. Your emotional support has been a constant source of strength, motivating me to overcome challenges and persevere through the various stages of this academic journey.

ABSTRACT

Particle breakage is one of the phenomena that poses challenges in soil behavior is the crushing of soil particles, which tends to occur under high-stress conditions induced by processes like pile driving, cone penetration testing, and large earth-fill dams. It also plays an important role in causing excessive ground subsidence during dam construction, long-runout landslides triggered by earthquakes, and free-fall during pile foundation installation. The phenomenon of particle crushing leads to significant volume change and altered mechanical properties of the soil, making it difficult to accurately capture using conventional constitutive models.

Conventional constitutive models face difficulties in precisely capturing the intricate behavior of these soils, hindering the reliability of geotechnical analysis and design. This study introduces a novel constitutive model specifically designed for crushable soils. The proposed model incorporates fundamental mechanisms of particle breakage, rearrangement, and volume change to provide a comprehensive representation of their behavior. Various past experimental data, including triaxial compression, oedometer, and direct shear tests were utilized to calibrate the model parameters.

Numerical simulations were then performed to validate the model against experimental results. The results demonstrate the model's ability to accurately reproduce stress-strain relationships and volumetric behavior of crushable soils under various loading conditions. This model presents a significant advancement in geotechnical engineering, offering enhanced accuracy in predicting soil structure response and improving safety in geotechnical designs. Further research is warranted to explore additional complexities and refine the model's capabilities. Ultimately, the proposed constitutive model contributes to advancing geotechnical engineering practice, ensuring reliable and robust analysis for crushable soils.

TABLE OF CONTENTS

LIST OF FIGURES

LIST OF TABLES

CHAPTER 1
INTRODUCTION

1.1 RESEARCH BACKGROUND

In the geotechnical engineering field, understanding the mechanical behavior of soil is crucial when it comes to designing safe and reliable structures. Soil, being a complex and heterogeneous material, exhibits a wide range of behaviors under varying load conditions. Accurate modeling of soil behavior is essential for predicting the response of soil structures and ensuring their stability.

Particle breakage is one of the phenomena that poses challenges in soil behavior. It tends to occur under high-stress conditions induced by processes like pile driving, cone penetration testing, and large earth-fill dams (Lee and Farhoomand, 1967; Russell and Khalili, 2002). The crushing of particles also plays an important role in causing excessive ground subsidence during dam construction (Oldecop et al, 2001), long-runout landslides triggered by earthquakes (Wang et al, 2002; Zhang et al, 2019) and free-fall during pile foundation installation (Senders et al, 2013). The phenomenon of particle crushing leads to significant volume change and altered mechanical properties of the soil, making it difficult to accurately capture using conventional constitutive models.

Experimental evidence in recent decades has contributed to the understanding of how particle crushing occurs. Some researchers have established a correlation between applied stress and grading evolution (Coop and Lee, 1993; Hardin, 1985; Hyodo et al, 2002; Yasufuku et al, 1991; Luzzani and Coop 2002), while others have emphasized the contribution of deformation (strain) to the generation of crushing through cyclic loading tests (Hyodo et al, 2002) and ring shear tests (Coop et al, 2004). Additionally, the relationship between total energy dissipation and grading variation has also been discussed (Miura et al, 1984; McDowell et al, 2002; Lade et al, 1996). Experimental findings indicate the impact of compression and shearing on particle grading, with Hardin (1985) observing a correlation between particle breakage and stress levels, and Coop et al. (2004) highlighting the influence

of strain levels on crushing. Furthermore, the effect of cyclic loading has been observed, leading to a higher degree of particle crushing (Wu et al, 2020).

Conventional constitutive models have made progress in describing the behavior of various soil types, but they often struggle to accurately capture the behavior of crushable soils. Nevertheless, in recent times, there have been significant advancements resulting in the development of particle crushing models. Pestana & Whittle (1995) introduced an elastoplastic model treating crushing as particle damage, but it did not explicitly consider grading change, hindering a comprehensive understanding. Kikumoto et al. (2010) addressed grading change using a grading index and critical state soil mechanics, but their model only considered stress history, neglecting continuous deformation. Einav (2007a; 2007b) proposed an energy-based breakage mechanics model, which considers breakage energy, applied stress, and strain in the evolution of crushing. Notably, the interpretation of hardening in this model differs from the classical critical state soil mechanics approach. Daouadji & Hicher (2009) developed a critical state-based model for crushable granular material, considering both strain and stress separately for compression and shearing.

In this study, a constitutive model for crushable soil with a rational evolution law of grading is proposed and validated. It is proposed after analyzing and understanding the phenomena of crushing through experiments and past studies. The evolution of grading considers both stress and strain history in the framework of the elastoplastic model. The model introduces a state boundary surface, representing the upper limit of specific volume, which accounts for the impact of crushing on the mechanical response regardless of compression or shearing. The subloading surface concept is also applied to the model to consider the packing density on stress-strain characteristics. Utilizing the proposed model, a series of triaxial compression tests on Akadama soil, considering a wide range of stress states, loading paths, and strain rates were simulated to validate the model. After validating the model, parametric studies were conducted to learn about the parameter behavior and model responses.

1.2 RESEARCH OBJECTIVES

The primary objective of this research is to develop a rational constitutive model for soil considering particle crushing effect. To aim for the main objectives, the following steps will be followed.

1. To explore the crushing phenomena through past experimental proof.
2. To propose the constitutive model for soil with rational evolution law of grading.
3. To investigate the utilization of the model through parametric studies.

1.3 FRAMEWORK OF THE DISSERTATION

The contents of each chapter in the dissertation are summarized as follows.

Chapter 1 INTRODUCTION

This chapter concludes the background of the research, objectives, and the framework of the dissertation.

Chapter 2 LITERATURE REVIEW OF PARTICLE CRUSHING PHENOMENA

This chapter includes past research activities related to particle crushing phenomena, the development of grading index parameters, and the factors affecting changing grading through the past experimental evidence of crushable soils.

Chapter 3 ELASTOPLASTIC CONSTITUTIVE MODEL CONSIDERING PARTICLE CRUSHING

In this chapter, the explanation of how the model considering particle crushing is developed. The previous model and how the improvement has been introduced to the model are also included.

Chapter 4 MODEL VALIDATION FOR CRUSHABLE SOILS

In this chapter, the proposed model is validated by the experimental data of Akadama soil provided. A parametric study was also provided to describe the model characteristics and the crushable soil itself.

Chapter 5 CONCLUDING REMARKS AND FUTURE RESEARCH

Chapter 5 includes a summary of all the research activities and suggestions for findings and conclusions.

CHAPTER 2
LITERATURE REVIEW OF PARTICLE CRUSHING PHENOMENA

2.1 DEFINITION OF PARTICLE CRUSHING

In soil mechanics, particle crushing denotes the phenomenon wherein soil breaks down or fractures when subjected to applied stress. When a load is applied to a soil mass, the individual particles encounter forces that may lead to their deformation and subsequent fragmentation into smaller fragments. This phenomenon is particularly relevant in granular soils, including sands and gravels.

A type of soil that is susceptible to particle crushing or fragmentation under applied stress is called crushable soil. Carbonate sands and volcanic soil are examples of soil types with a high degree of crushability (Figure 2-1). Volcanic soils are generally composed of various minerals, including volcanic ash, pumice, and other volcanic rock fragments. Depending on the specific type of volcanic soil, the particles may have varying degrees of crushability. For example, volcanic ash can be relatively fine-grained and may experience particle crushing under stress. Carbonate sands are composed of carbonate minerals such as calcite or aragonite. The crushability of carbonate sands is generally lower than that of some granular soils like sands or gravels. However, carbonate sands can undergo crushing under certain stress conditions, particularly if they contain coarser particles.

These soils are composed of relatively coarse particles, and under applied stress, the individual grains may undergo crushing or fragmentation. The crushability of these soils is influenced by factors such as particle size, mineral composition, and the conditions under which the soil is loaded. It also can vary widely based on local geological conditions and the specific characteristics of the soil in each location.

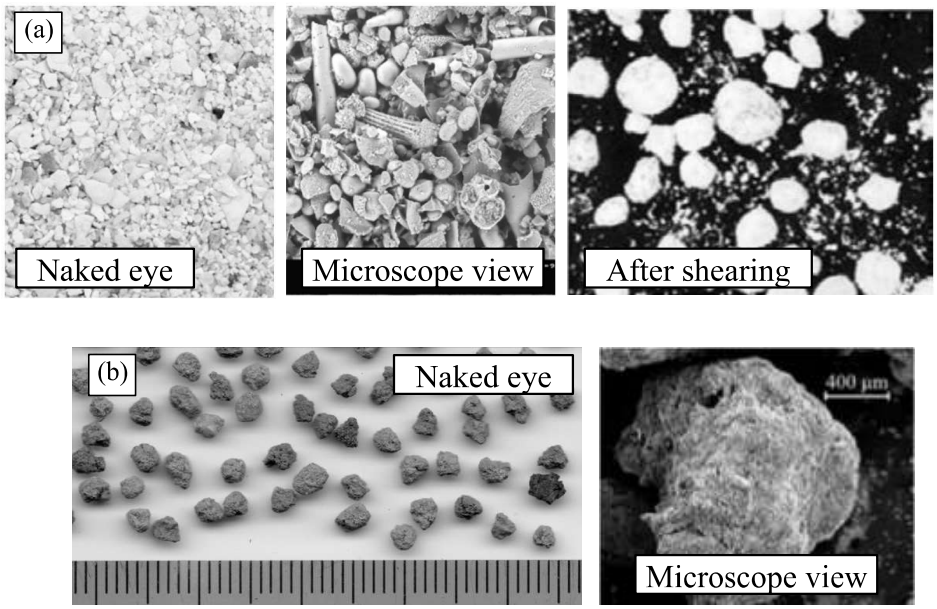

Figure 2-1 Example of crushable soils (a) Carbonate sand of North West Shelf, Australia (Senders et al, 2013); (b) Akadama soil

2.2 INDEX PARAMETER FOR PARTICLE CRUSHING

In order to describe the evolution of grading, we need an index to define the crushing degree. Some researchers use specific area as the index to define crushing degree (Hyodo et al, 2002). Specific surface area is often used as an index to define particle crushing because it provides a quantitative measure of the amount of surface area per unit mass of soil particles. As particles break down or fragment due to crushing, the total surface area of the particles increases.

Particle size distribution is also often used as an index to define particle crushing because changes in the distribution reflect alterations in the size range of soil particles due to crushing processes. Particle crushing leads to the production of finer particles as larger particles break down. The overall particle size distribution shifts towards smaller sizes as a result of crushing. By comparing the particle size distribution before and after loading, researchers can quantify the changes in particle sizes and use this information to assess the degree of particle crushing. This allows for comparative analyses across different soil samples and conditions. Hence,

numeral researchers have made efforts to propose effective grading indices based on particle size distribution.

The single-grading index B_{15} was introduced by Lee and Farhoomand (1967). B_{15} is the ratio of the 15 percent size of the soil, D_{15} before testing into the 15 percent size after testing. The 15 percent size was adopted because it is also the key size criterion used in the design of drains and filters.

$$B_{15} = \frac{D_{15i}}{D_{15a}} \tag{2-1}$$

Anticipated inaccuracies in B_{15} are likely to be magnified when dividing a smaller value (D_{15a}) by a larger value (D_{15i}), particularly when D_{15a} is considerably small due to significant breakage under high pressure or extensive deformation. Lade et al. (1996) pointed out the excessive sensitivity of the breakage index to minor fluctuations in the measured D_{15a} values and introduced a modified single-grading breakage index, denoted as B_{10}.

$$B_{10} = 1 - \frac{D_{10a}}{D_{10i}} \tag{2-2}$$

D_{10i} and D_{10a} is the effective particle size corresponding to 10% finer on PSD before and after the tests, respectively. Marsal (1967) introduced a single-grading index, B_g, defined as the maximum difference between the PSD curves before and after the test. This index can be described as follows.

$$B_g = \Delta P_{\max} \tag{2-3}$$

Similarly, Nakata et al. (1999) proposed a single-grading breakage index, denoted as B_f, which can be defined as follows.

$$B_f = 1 - P_0 \tag{2-4}$$

P_0 is the percentage of particles in current PSD that are smaller than the minimum particle size in the original sand.

The utilization of single-grading breakage index is unable to represent the crushing of grains of varying sizes comprehensively. To address the limitation of single-grading breakage indices, Hardin (1985) introduced an effective relative breakage index, B_r, as shown in Figure 2-2, which can be described as follows.

$$B_r = \frac{\mathrm{B}_t}{B_p} \tag{2-5}$$

B_t and B_p are total breakage and the breakage potential, respectively, and can be defined as follows.

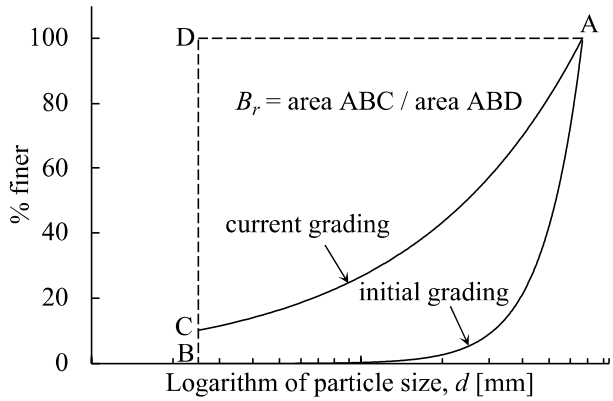

Figure 2-2 Definition of relative breakage, *Br*

The grading index, I_G was introduced by Muir Wood (2007) to give a simplified interpretation of the crushing state of the material. I_G is a scalar value ranging from 0 (indicating the unit grading) to 1 (indicating the limiting grading). Its computation involves determining the ratio of the area beneath the current grading curve to the total area, as depicted in Figure 2-3.

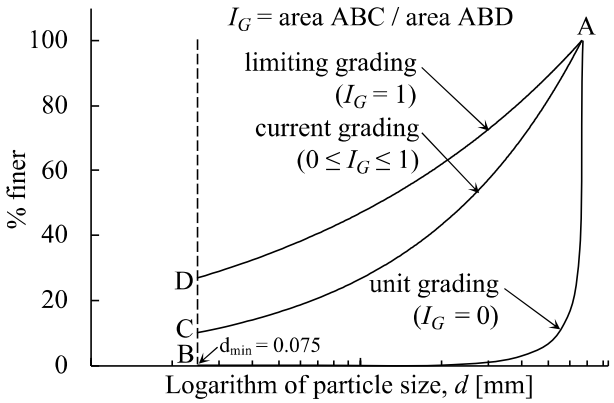

Figure 2-3 Definition of grading index, I_G

$$I_G = \frac{area\ ABC}{area\ ABOD} \tag{2-6}$$

2.3 FACTOR AFFECTING CHANGING OF GRADING – EXPERIMENTS OF CRUSHABLE SOILS

After defining the grading index to denote the grading change due to particle crushing, we need to know the key factors influencing this change. The majority of the researchers pay attention to the applied stress level. The magnitude and duration of the applied stress significantly influence the extent of particle crushing. Higher stress levels are likely to result in more significant changes in particle size distribution.

The triaxial tests on Dog's Bay sand conducted by Coop and Lee (2002) show the influence of the applied stress on the grading change of the soil. Higher stress levels result in more significant particle crushing. Different loading paths also result in distinct changes in particle size distribution. Notably, particle crushing caused by shearing is higher compared to compression (Figure 2-4).

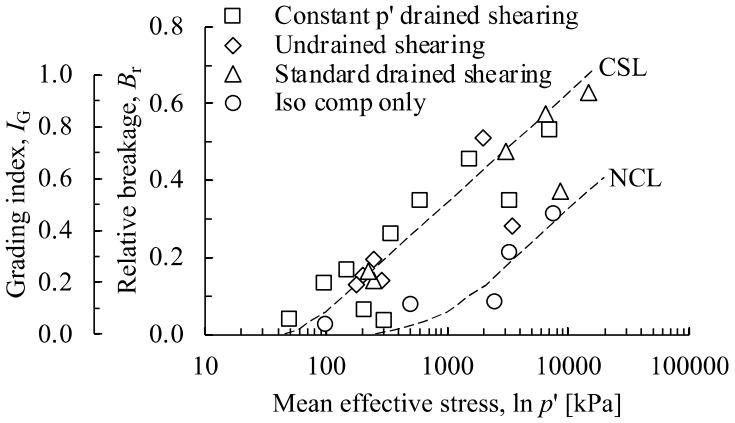

Figure 2-4 Particle breakage for isotropically compressed and sheared sand samples (after Coop and Lee 1993) (Luzzani and Coop 2002)

While applied stress primarily influences the evolution of grading in soils undergoing particle crushing, strain level is also involved in the overall mechanism of particle crushing. To investigate the effect of strain levels on particle crushing, Coop et al (2004) conducted ring shear tests on crushable soils. In a ring shear test, the soil sample is subjected to controlled and continuous shearing stress. This allows researchers to apply different levels of shear stress systematically, providing a controlled environment to study the soil's response to strain.

These tests were conducted on a wide range of stress and strain levels, as depicted in Figure 2-5. The tests were conducted by applying different shear stress levels and continuous shearing to large amounts of shear strain levels. The result indicates the increase of crushing degree with the increase of strain levels.

Other researchers also investigated the correlation between plastic work and crushability. Plastic work refers to the work done on a material during plastic deformation under the influence of applied stresses. The definition of plastic work can be seen in Equation (2-7). It is a combination of plastic strain and stress levels. In the work of McDowell et al. (2002) the correlation between plastic work and particle crushing can be seen in Figure 2-6.

$$W^P = \int dW^P = \int \left(p' d\varepsilon_v + q d\varepsilon_q\right) - \left(p' d\varepsilon_v^e + q d\varepsilon_q^e\right) \tag{2-7}$$

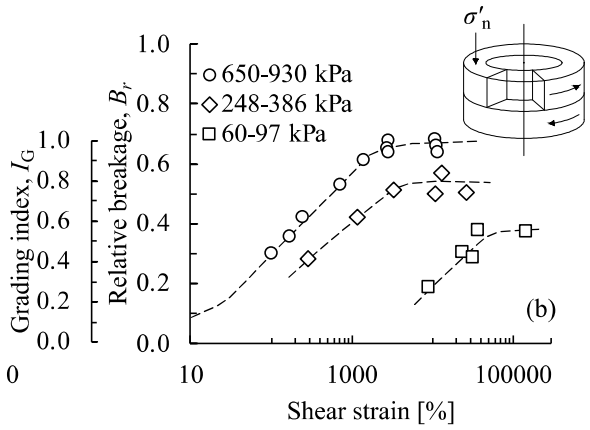

Figure 2-5 Evolution of relative breakage with different stress and strain level on ring shear test (replotted from Coop, et al., 2004)

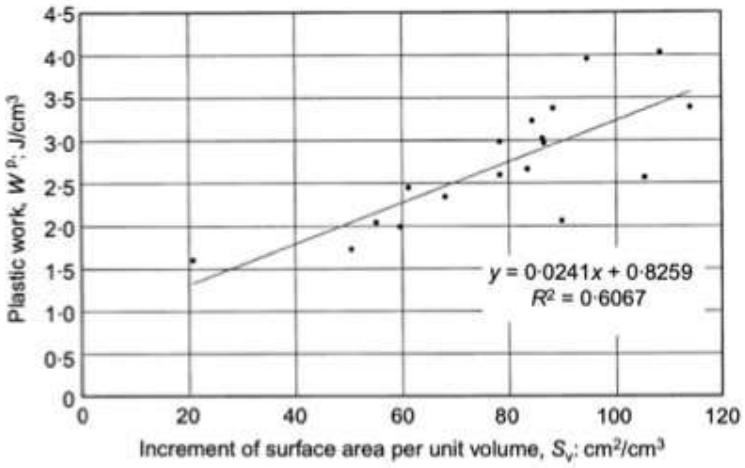

Figure 2-6 Correlation of plastic work with surface area (McDowell et al., 2002)

The type of loading conditions, whether it is static or cyclic loading, can affect the degree of particle crushing. Cyclic loading can lead to cumulative particle crushing over multiple loading cycles. Each cycle of loading and unloading may cause some degree of particle breakage, contributing to the overall crushability of the soil. Cyclic loading tests on Aio sand conducted by Hyodo et al. (2002) indicate that although the highest applied stress is comparatively low, the crushing depicted by the increase of surface area still happens. During liquefaction, even when the

applied stress level is relatively low, significant crushing represented by the increase in surface area can be found.

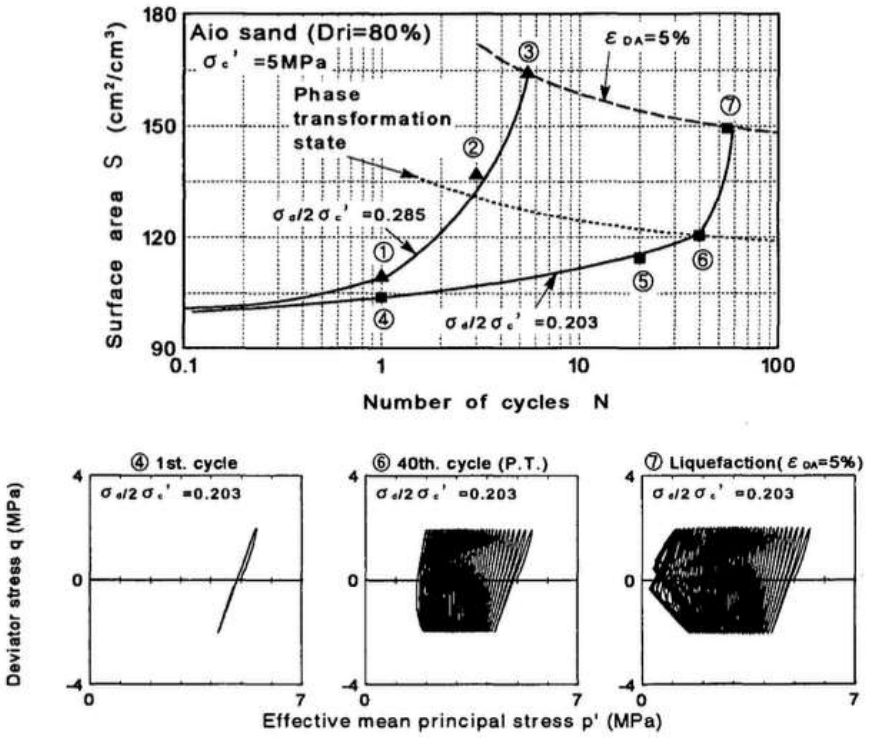

Figure 2-7 Correlation between cyclic stress path

CHAPTER 3
ELASTOPLASTIC CONSTITUTIVE MODEL CONSIDERING PARTICLE CRUSHING

3.1 MODELING THE EVOLUTION OF GRADING INDEX

Once the grading index to be used is determined, the subsequent step involves clarifying its evolution and identifying the factors influencing it. To establish a rational evolution law, it is necessary to examine experimental evidence and prior studies. Previous research has predominantly emphasized the influence of stress levels. Hardin (1985) introduced a hyperbolic correlation between relative breakage (B_r) and breakage effective stress (σ_b), drawing upon experiments conducted by Lee and Farhoomand (1967). The relationship can be expressed as follows.

$$B_r = \frac{\left(\frac{\sigma_b}{\sigma_r}\right)^{n_b}}{1+\left(\frac{\sigma_b}{\sigma_r}\right)^{n_b}} \tag{3-1}$$

The material constants σ_r and n_b correspond to the breakage reference stress and breakage number, respectively. Expressing σ_b in terms of mean effective stress, p' and deviator stress, q, we have the following formulation.

$$\sigma_b = p'\left[1+\frac{2\sqrt{2}}{3}\left(\frac{q}{p'}\right)^3\right] \approx p'[1+\eta^3] \tag{3-2}$$

The triaxial tests conducted by Coop and Lee (1993) on Dog's Bay sand (as depicted in Figure 2-4) provide evident results regarding the impact of increasing stress levels on the increase of crushing levels. Furthermore, this experiment highlights the disparity in the extent of crushing induced by isotropic compression and shearing. Specifically, shearing leads to a greater degree of crushing compared to compression.

The triaxial test has limitations in reaching high strain levels, which hinders a clear understanding of the significant influence of strain levels on soil particle crushing. The result will become less accurate as large strains are approached. To investigate this in more depth this matter, Coop et al. (2004) conducted a series of ring shear tests on the carbonate sand, Dog's Bay sand. Ring shear tests enable soil samples to be sheared to higher displacements, facilitating an investigation into the impact of strain level on grading evolution.

These tests were conducted on a wide range of stress and strain levels, as depicted in Figure 2-5 (a). Different applied vertical stresses were employed, with the sample subjected to small displacements up to very large displacements. The results revealed the existence of a maximum grading index, beyond which no further crushing occurs. This asymptotic state is contingent on the stress level. As the strain level increases, the grading strives to approach the asymptotic state for each stress level. This demonstrates that the evolution of grading cannot be adequately described by stress state alone. Based on this result, we can define an exponential function of the maximum grading index (I_G^{max}) as a function of normal effective stress, σ_n' (Figure 2-5 (b)).

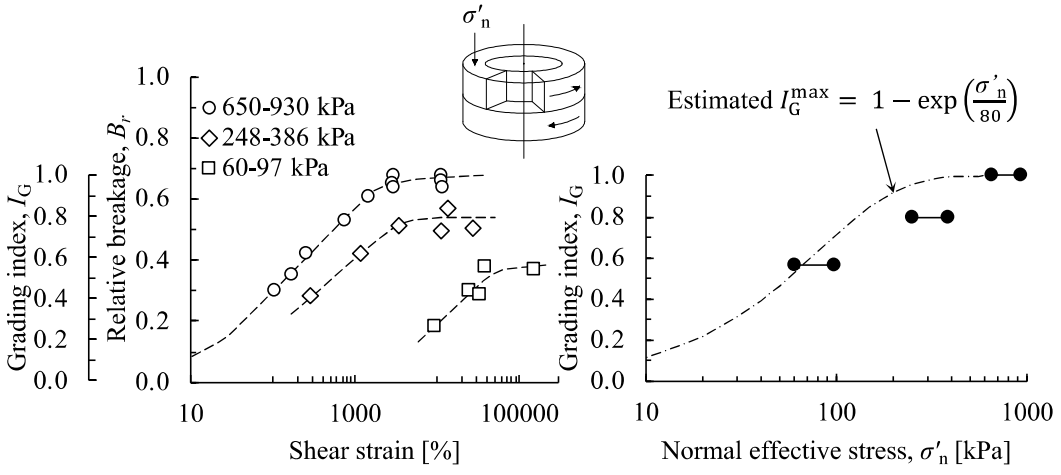

Figure 3-1 Evolution of relative breakage with different stress and strain level on ring shear test (replotted from Coop, et al., 2004)

In their study, Kikumoto et al. (2010) explored the impact of stress on particle crushing. The author noted that the changes in grading resulting from particle crushing should be related to stress and strain histories, as they are linked to plastic deformation and contribute to the ongoing evolution of grading toward the critical state, irrespective of stress levels. Eventually, the evolution with respect to stress levels, incorporating the crushing surface and maximum stress history, was chosen due to the significant influence of stress levels on the increment of the I_G value. However, evaluating crushing based on stress levels has certain drawbacks, particularly in cases where the stress levels remain low concurrently with an increase in plastic strain.

Based on those ideas and evidence from the experiments, we come up with the evolution law of I_G which considers the effect of stress and strain levels. First, we defined σ_b as the crushing stress that is defined by the current stress state that is defined by mean effective stress, p' and deviator stress, q (Figure 3-2 (a)). σ_b is formulated as follows.

$$\sigma_b = p' \left[1 + k_\eta \left(\frac{q}{p'} \right)^3 \right] \tag{3-3}$$

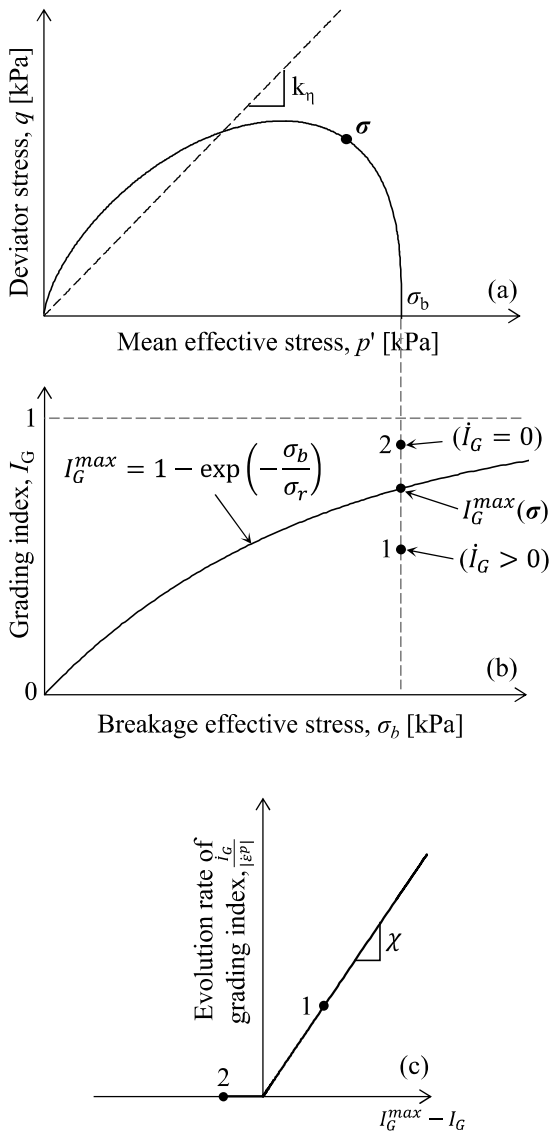

Figure 3-2 (a) Breakage effective stress as the function of mean effective stress p' and deviator stress q; (b) Distance of I_G to I_G^{max} based on breakage effective stress σ_b; (c) Evolution of IG with parameter constant for the rate of crushing, χ

Crushing stress, σ_b acts as a crushing surface that crosses the current stress state, $\boldsymbol{\sigma}$. The shape of the crushing stress is characterized by the slope of k_η. k_η is a parameter defining the effect of shearing on the crushing of sand particles. This is to differentiate how each different type of sand reacts to stress that causes the breakage of particles.

Using σ_b, the maximum level of grading index I_G, I_G^{max} is determined. I_G^{max} is the current maximum grading index that can be attained (Figure 3-2 (b)). We always check the evolution of I_G at the current stress state based on the current I_G^{max}. The relative location of I_G determines the rate of evolution of I_G. There are two conditions. If the current I_G value is below the current I_G^{max} value (state 1), the grading index will try to reach the I_G^{max} due to the plastic strain development. However, in certain cases, it is possible for having I_G value the same or larger compared to the I_G^{max} value. This can occur due to previous high-stress applications that resulted in significant particle crushing. When unloading the soil, there is a potential for the I_G to exceed the current I_G^{max} (state 2). Under this situation, we do not have any further crushing ($\dot{I}_G = 0$). The formulation of I_G^{max} is expressed as follows.

$$I_G^{max}(p', q) = 1 - \exp\left(-\frac{\sigma_b}{\sigma_r}\right) \tag{3-4}$$

σ_r is a material constant defining crushing stress resistance. As σ_b is defined by mean effective stress p', and deviator stress, q, the crushing development due to compression and shearing can be differentiated. The exponential form of I_G^{max} ensures the monotonic increase of I_G^{max} with the increase of crushing stress, σ_b until reaching the asymptotic state (Kikumoto et al., 2010). With a high-stress level, I_G^{max} should be able to reach 1 which is the limiting grading.

Finally, the evolution of I_G is calculated by checking the distance between the current I_G value to the current I_G^{max}.

$$\dot{I}_G = \chi\langle I_G^{max} - I_G\rangle|\dot{\varepsilon}^p| \tag{3-5}$$

χ is a parameter to define the rate of crushing. This depends on the material properties that will affect the crushability of the soil particles such as particle shape and strength. The evolution of IG is determined by plastic strain increment, $|\dot{\varepsilon}^p|$ as the irreversible part of the strain that is used to account for the irreversibility of crushing that occurs to the soil. I_G will continuously increase until reaching

I_G^{max} when plastic strain is generated. Once I_G reaches I_G^{max}, there will be no further crushing generated. With this equation, the evolution of the grading index I_G can be described with the effect of strain and stress level (Figure 3-2 (c)).

3.2 FORMULATION OF CONSTITUTIVE MODEL CONSIDERING PARTICLE CRUSHING

In 2010, Kikumoto et al. developed a model for soils considering the effect of changing grading based on the Severn-Trent sand model incorporating Mohr-Coulomb failure (Gajo & Muir Wood, 1999). Nguyen & Kikumoto (2018) further developed an improved model to describe the effect of crushing on compression and shearing in a unified manner. This model will be used to explore the cyclic behavior of crushable soils.

3.2.1 Critical state, state parameters, and state boundary surface for sand

There exists a unique locus of asymptotic, critical states sought by sand when it is sheared, which can be expressed in terms of specific volume and mean effective stress (Figure 3-3). A usual form of the critical state line (CSL) for sand (e.g., Gajo and Muir Wood, 1999) is given as linear in a semi-logarithmic $\ln p'$-v plane as follows.

$$v_{cs} = \Gamma - \lambda \ln\left(\frac{p'}{p_a}\right) \tag{3-6}$$

where Γ defines the specific volume at the critical state under $p' = p_a$, λ is the slope of the CSL in the semi-logarithmic $\ln p'$-v plane, and $p'\left(=\frac{\mathrm{tr}\,\boldsymbol{\sigma}'}{3}\right)$ is the mean stress and stress ratio given by the effective stress tensor $\boldsymbol{\sigma}'(=\boldsymbol{\sigma} - u_w\mathbf{1})$.

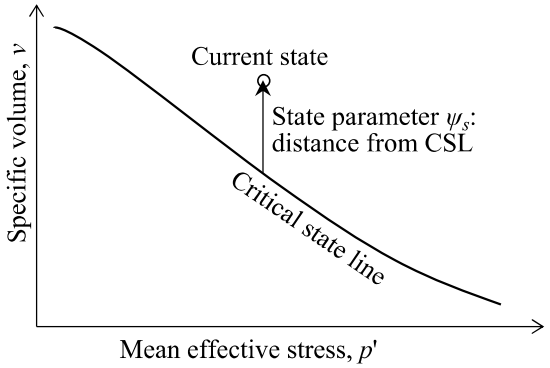

Figure 3-3 Critical state line in p'-v plane

Having identified a CSL, the state parameter for sand, ψ_s (Been and Jefferies, 1985), can be used as the volumetric distance of the current specific volume, v, from the CSL at the current mean effective stress (Figure 3-4).

$$\psi_s = v - v_{cs} \tag{3-7}$$

The available strength, η_u, is assumed to be a variable dependent on the state parameter, ψ.

$$\eta \leq \eta_u(\psi_s) \tag{3-8}$$

$\eta_u(\psi_s)$ is a monotonic decreasing function of the state parameter, ψ_s which bounds by the critical state stress ratio, M, when the state parameter, ψ_s is zero. Gajo and Muir Wood (1999) proposed a simple linear relationship between the available strength, η_u and the state parameter, ψ_s.

$$\eta_u(\psi) = \mathrm{M}(1 - k\psi_s) \tag{3-9}$$

In the proposed model, a nonlinear relationship is applied.

$$\eta_u(\psi) = \mathrm{M}\sqrt{2^{1-k\psi_s} - 1} \tag{3-10}$$

where M and k is a positive constitutive parameter.

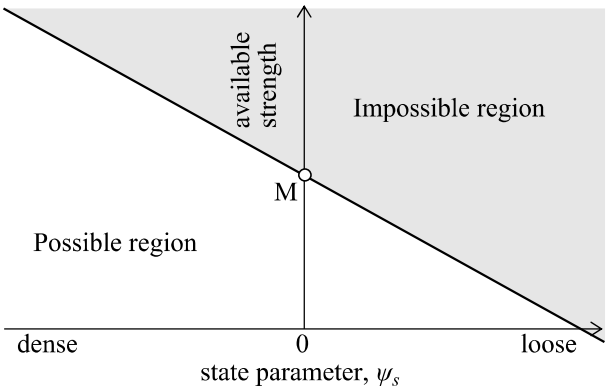

Figure 3-4 Strength of sand as a function of state parameter

The available strength, η_u, is a threshold of the impossible and possible regions. Substituting Eqs. (3-6) and (3-7) in (3-8) an alternative expression for Eq. (3-8) is derived as the upper threshold of the specific volume, v_u, for sand.

$$v \le v_u(p',\eta) = \underbrace{\left(\frac{1}{k}+\Gamma\right)}_{N} - \lambda \ln\frac{p'}{p_a} - \frac{1}{k}\underbrace{\frac{\ln\left\{1+\left(\frac{\eta}{M}\right)^2\right\}}{\ln 2}}_{\zeta(\eta)} \tag{3-11}$$

Here, the upper specific volumes under $p' = p_a$ at isotropic stress ($\eta = 0$) and at critical state stress ratio ($\eta = M$) are $N\left(=\frac{1}{k}+\Gamma\right)$ and Γ, respectively. From Eqs. (3-8) and (3-11), it is known that an essential element of the critical state model for sand is the existence of a unique state boundary surface (SBS) that separates the possible and impossible states in the space of the effective stress p', stress ratio η, and specific volume v. The SBS plays a central role in describing soil behavior in the proposed model.

3.2.2 An elastoplastic model considering particle crushing of sands

To be able to incorporate the effect of changing grading, the SBS given by Eq. (3-11) needs to be extended. The particle crushing causes the soils to become more compressive. To integrate this assumption, the SBS for crushable soils is assumed to shift downward in the plane of specific volume, v versus logarithmic of mean effective stress, p'. The downward shift is controlled by the state parameter $\Psi(I_G)$ which has been explained in the previous subchapter. $\Psi(I_G)$ is a non-negative

variable to represent the volumetric distance between the SBS of the current state and the fully crushed one (Figure 3-5). Therefore, the specific volume on the SBS for sands considering particle crushing can be defined as follows.

$$v \le v_u(p', \eta, I_G) = \underbrace{\left(\frac{1}{k} + \Gamma\right)}_{\mathrm{N}} - \lambda \ln \frac{p'}{p_a} - \frac{1}{k} \underbrace{\frac{\ln\left\{1 + \left(\frac{\eta}{\mathrm{M}}\right)^2\right\}}{\ln 2}}_{\zeta(\eta)} + \Psi(I_G) \qquad (3\text{-}12)$$

State parameter Ψ is simply defined as

$$\Psi = \xi(1 - I_G) \qquad (3\text{-}13)$$

ξ is a constant to specify the distance between the state boundary surface for I_G is equal to 0, where crushing has not occurred, and the state boundary surface when the soil particles are fully crushed ($I_G = 1$). For the stress-strain relationship, an additive decomposition of the total strain rate tensor is assumed as follows.

$$\dot{\boldsymbol{\varepsilon}} = \dot{\boldsymbol{\varepsilon}}^e + \dot{\boldsymbol{\varepsilon}}^p \qquad (3\text{-}14)$$

where $\dot{\boldsymbol{\varepsilon}}^e$ and $\dot{\boldsymbol{\varepsilon}}^p$ are the elastic and plastic strain rate tensors, respectively. Elastic volumetric behavior is assumed to follow a conventional, linear relationship in the semi-logarithmic plane of $\ln p'$ and v. Thus, an elastic part of the variation in the specific volume, dv^e, is given as follows.

$$dv^e = -\kappa \frac{dp'}{p'} \qquad (3\text{-}15)$$

where κ is the swelling index that represents the slope of the isotropic unloading (swelling) line in the $\ln p'$-v plane. The nonlinear elastic bulk modulus can be defined as follows.

$$K = \frac{v_0}{\kappa} p' \qquad (3\text{-}16)$$

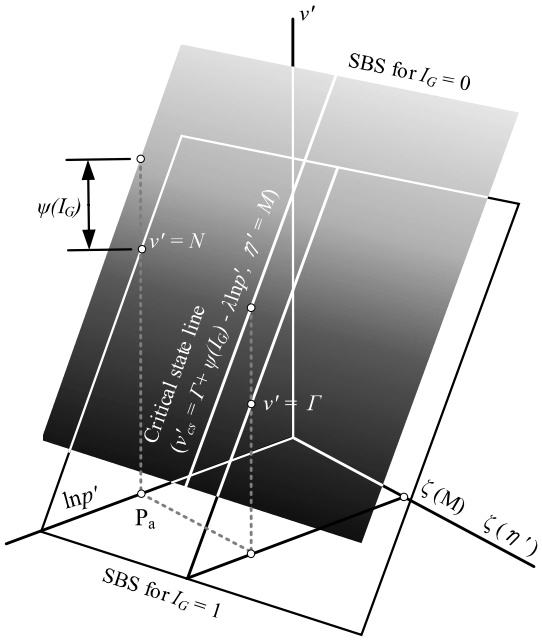

Figure 3-5 Upper limit of specific volume of crushable soils defined by SBS as a function of p', q, and ψ

Assuming that Poisson's ratio ν_e is constant, the shear modulus G is:

$$G = \frac{3K(1-2\nu_{\mathrm{e}})}{2(1+\nu_{\mathrm{e}})} \tag{3-17}$$

Thus, the incremental isotropic elastic relationship is:

$$\dot{\boldsymbol{\sigma}}' = \underbrace{\left\{K\mathbf{1}\otimes\mathbf{1} + 2G\left(\boldsymbol{I} - \frac{1}{3}\mathbf{1}\otimes\mathbf{1}\right)\right\}}_{\boldsymbol{D}^{\mathrm{e}}} : \dot{\boldsymbol{\varepsilon}}^{\mathrm{e}} \tag{3-18}$$

where $\dot{\boldsymbol{\sigma}}'$ is the rate of effective stress tensor and $\boldsymbol{D}^e$ is the elastic stiffness tensor.

Plastic volumetric deformation is exhibited so that the specific volume never exceeds the SBS. Therefore, the bounding surface, $\tilde{f}$, for the proposed model is defined as follows.

$$\tilde{f} = v - v_u (\leq 0) \tag{3-19}$$

where $\tilde{f}$ is a non–positive function that increases to zero when the state of the soil approaches the SBS. $\tilde{f}$ is equivalent to the yield function of a classical critical state model, modified Cam-clay. However, classical models predict purely elastic behavior within the yield surface, whereas actual sand exhibits elastoplastic irreversible deformation below the SBS. Therefore, we assume a yield surface within the bounding surface to describe a smooth transition from elastic to plastic behavior. Accordingly, a margin to the normal yielding state is scaled simply by a volumetric difference, Ω, from the current specific volume to the specific volume on the SBS under the current mean effective stress p' and deviator stress q.

$$\Omega = v_{\mathrm{sbs}} - v \ (\geq 0) \tag{3-20}$$

Based on Eqs. (3-19) and (3-20), the yield function can be derived as:

$$f = v - v_u + \Omega \equiv 0 \tag{3-21}$$

It should be noted that the function f is identically equal to zero. The variables are hereafter denoted as (v_0, p_0', η_0) and (v, p', η, Ω) at the initial and current states, respectively. The variation in specific volume from the initial state to the current state, $\Delta v(= v - v_0)$, can be decomposed into elastic and plastic variations in the specific volume, Δv^e and Δv^p.

$$\Delta v(= v - v_0) = \underbrace{\left(-\kappa \ln \frac{p'}{p_0'}\right)}_{\Delta v^e} + \underbrace{\left(-v_0 \varepsilon_{\mathrm{v}}^p\right)}_{\Delta v^p} \tag{3-22}$$

where $\varepsilon_{\mathrm{v}}^p (= \mathrm{tr}\boldsymbol{\varepsilon}^{\mathbf{p}})$ denotes the plastic volumetric strain. Using Eq. (3-11) and Eq. (3-20), the yield function given by Eq. (3-21) can be rewritten as:

$$\begin{aligned} f\left(p', \eta, \varepsilon_{\mathrm{v}}^p, \Omega\right) = & \left(v_0 - \kappa \ln \frac{p'}{p_0'} - v_0 \varepsilon_{\mathrm{v}}^p\right) \\ & - \left(N - \lambda \ln \frac{p'}{p_{\mathrm{a}}} - (N - \Gamma)\zeta(\eta')\right) + \Omega - \Psi \end{aligned} \tag{3-23}$$

Substituting $f\left(p_0', \eta_0, \varepsilon_{v0}^p (=0), \Omega_0\right) = 0$ into Eq. (3-23), we derive:

$$f\left(p', \eta, \varepsilon_v^p, \Omega\right) = \underbrace{(\lambda - \kappa) \ln \frac{p'}{p_0'} + (N - \Gamma)\{\zeta(\eta) - \zeta(\eta_0)\}}_{F(\boldsymbol{\sigma})} - \underbrace{\left\{v_0 \varepsilon_v^p - (\Omega - \Omega_0)\right\}}_{H\left(\varepsilon_v^p, \Omega\right)} \tag{3-24}$$

Assuming the normality condition (associated flow), the direction of the plastic strain rate, $\dot{\boldsymbol{\varepsilon}}^p$, is:

$$\dot{\boldsymbol{\varepsilon}}^p = \dot{\Lambda} \frac{\partial f}{\partial \boldsymbol{\sigma}'} \tag{3-25}$$

As the soil does not exhibit any dilation in the critical state $\eta = \mathrm{M}$, the following condition is obtained.

$$\left.\frac{\partial f(p', q)}{\partial p'}\right|_{\eta = M} = 0 \tag{3-26}$$

Substituting Eqs. (3-12) and Eq. (3-24), Eq. (3-26) can be reduced to:

$$\frac{1}{k} = N - \Gamma = \ln 2\,(\lambda - \kappa) \tag{3-27}$$

Finally, the yield function becomes:

$$f\left(p', \eta, \varepsilon_v^p, \Omega\right) = \underbrace{(\lambda - \kappa) \ln \frac{p' \left\{1 + \left(\frac{\eta}{M}\right)^2\right\}}{p_0' \left\{1 + \left(\frac{\eta_0}{M}\right)^2\right\}}}_{F(\boldsymbol{\sigma}')} - \underbrace{\left\{v_0 \varepsilon_v^p - (\Omega - \Omega_0) + (\Psi - \Psi_0)\right\}}_{H\left(\varepsilon_v^p, \Omega, \Psi\right)} \equiv 0 \tag{3-28}$$

where $F(\boldsymbol{\sigma}')$ is the yield stress function and $H\left(\varepsilon_v^p, \Omega\right)$ is the isotropic hardening function. The function f is identically equal to zero. The function f satisfies the

necessary condition that the yield function is a non-positive convex function of the stress $\boldsymbol{\sigma}'$ and the hardening parameters ε_v^p and Ω.

In any loading path, the Kuhn-Tucker conditions (Kuhn and Tucker, 1951) must be satisfied.

$$f \leq 0;\ \dot{\Lambda} \geq 0;\ \dot{\Lambda} f = 0 \tag{3-29}$$

As the yield function applied in the proposed model (Eq. (3-20)) is identically equal to zero, the loading condition reduces to:

$$\dot{\Lambda} \geq 0 \tag{3-30}$$

where $\dot{\Lambda} = 0$ indicates elastic behavior (neutral or unloading) and $\dot{\Lambda} > 0$ indicates plastic deformation (loading). When soil exhibits elastoplastic deformation, the consistency condition, that is the time derivative of the yield function $f\left(\boldsymbol{\sigma}', \varepsilon_{\mathrm{v}}^{\mathrm{p}}, \Omega, \Psi\right)$ equals zero, must be satisfied.

$$\dot{f} = \frac{\partial f}{\partial \boldsymbol{\sigma}'} : \dot{\boldsymbol{\sigma}}' + \frac{\partial f}{\partial \varepsilon_{\mathrm{v}}^{\mathrm{p}}} \dot{\varepsilon}_{\mathrm{v}}^{\mathrm{p}} + \frac{\partial f}{\partial \Omega} \dot{\Omega} + \frac{\partial f}{\partial \Psi} \dot{I}_G \equiv 0 \tag{3-31}$$

The hardening rule for the plastic volumetric strain, $\varepsilon_{\mathrm{v}}^{\mathrm{p}}$, is:

$$\frac{\partial f}{\partial \varepsilon_{\mathrm{v}}^{\mathrm{p}}} \dot{\varepsilon}_{\mathrm{v}}^{\mathrm{p}} = -v_0 \dot{\Lambda} \mathrm{tr} \frac{\partial f}{\partial \boldsymbol{\sigma}'} \tag{3-32}$$

As Ω is the parameter scaling of the volumetric distance from the current state to the normal yield (bounding) surface, it must decrease with the development of plastic deformation and converge to zero. Consequently, when soil exhibits plastic deformation (loading), a simple law enabling this evolution of Ω can be defined as:

$$\frac{\partial f}{\partial \Omega} \dot{\Omega} = -v_0 \omega \Omega |\Omega| \left\| \dot{\boldsymbol{\varepsilon}}^{\mathrm{p}} \right\| \quad \left(\dot{\Lambda} > 0\right) \tag{3-33}$$

where ω is a parameter that controls the rate of the evolution of Ω.

If the soil exhibits purely elastic deformation (unloading or neutral), the consistency condition (Eq. (3-23)) still needs to be satisfied as the yield function, f, is identically equal to zero. Therefore, the evolution law of Ω in unloading or neutral conditions is:

$$\dot{\Omega} = -\frac{\partial f}{\partial \boldsymbol{\sigma}'} : \dot{\boldsymbol{\sigma}}' \quad \left(\dot{\Lambda} = 0\right) \tag{3-34}$$

From Eqs. (3-14), (3-18), (3-25), (3-31), (3-32), and (3-33),the magnitude of the plastic strain rate, $\dot{\Lambda}$, is derived as:

$$\dot{\Lambda} = \langle \frac{\frac{\partial f}{\partial \boldsymbol{\sigma}'} : \boldsymbol{D}^{\mathrm{e}} : \dot{\boldsymbol{\varepsilon}}}{M^p + \frac{\partial f}{\partial \boldsymbol{\sigma}'} : \boldsymbol{D}^{\mathrm{e}} : \frac{\partial f}{\partial \boldsymbol{\sigma}'}} \rangle \tag{3-35}$$

where M^p is the plastic modulus defined as follows.

$$M^p = v_0 \mathrm{tr} \frac{\partial f}{\partial \boldsymbol{\sigma}'} + v_0 \omega \Omega |\Omega| \left\| \frac{\partial f}{\partial \boldsymbol{\sigma}'} \right\| - \xi (\chi (I_G^{max} - I_G) \left\| \frac{\partial f}{\partial \boldsymbol{\sigma}'} \right\| \tag{3-36}$$

Finally, the rate form of the elastoplastic stress-strain relationship can be defined as:

$$\dot{\boldsymbol{\sigma}}' = \boldsymbol{D}^{\mathrm{e}} : \dot{\boldsymbol{\varepsilon}} - \langle \frac{\frac{\partial f}{\partial \boldsymbol{\sigma}'} : \boldsymbol{D}^{\mathrm{e}} : \dot{\boldsymbol{\varepsilon}}}{M^p + \frac{\partial f}{\partial \boldsymbol{\sigma}'} : \boldsymbol{D}^{\mathrm{e}} : \frac{\partial f}{\partial \boldsymbol{\sigma}'}} \rangle \boldsymbol{D}^{\mathrm{e}} : \frac{\partial f}{\partial \boldsymbol{\sigma}'} \tag{3-37}$$

When the rate of the plastic multiplier $\dot{\Lambda}$ is positive, the rate form of the elastoplastic stress-strain relationship is converted to:

$$\dot{\boldsymbol{\sigma}}' = \underbrace{\left(\boldsymbol{D}^{\mathrm{e}} - \frac{\boldsymbol{D}^{\mathrm{e}} : \frac{\partial f}{\partial \boldsymbol{\sigma}'} \otimes \frac{\partial f}{\partial \boldsymbol{\sigma}'} : \boldsymbol{D}^{\mathrm{e}}}{M^p + \frac{\partial f}{\partial \boldsymbol{\sigma}'} : \boldsymbol{D}^{\mathrm{e}} : \frac{\partial f}{\partial \boldsymbol{\sigma}'}} \right)}_{\boldsymbol{D}^{\mathrm{ep}}} : \dot{\boldsymbol{\varepsilon}} \tag{3-38}$$

The outline of the model can be seen in Figure 3-6.

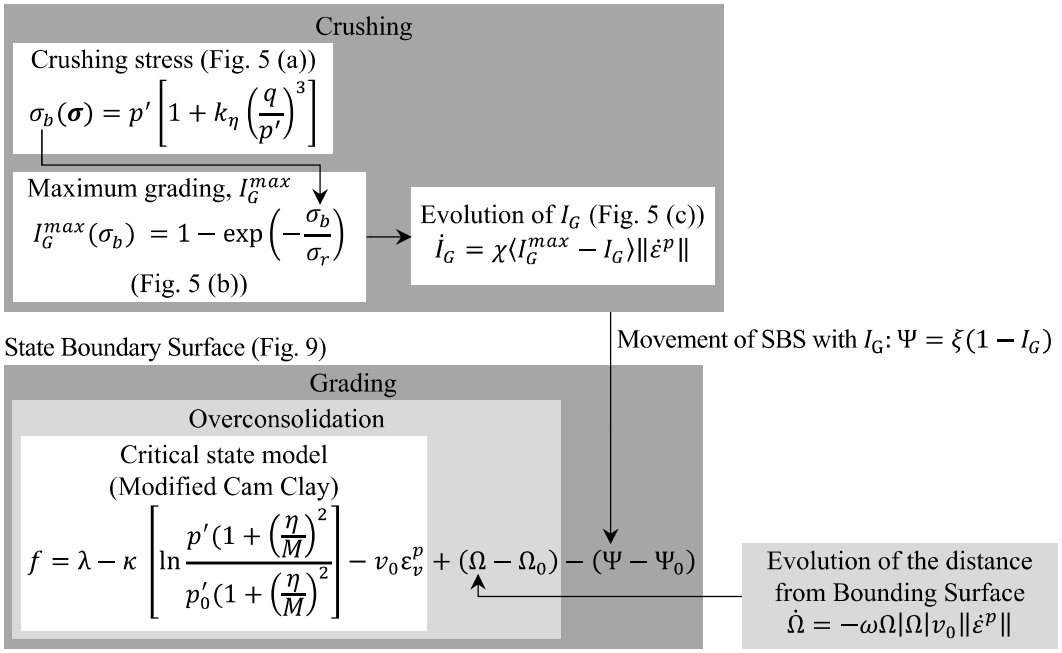

Figure 3-6 Outline of the model for crushable sands

CHAPTER 4
MODEL VALIDATION FOR CRUSHABLE SOILS

4.1 PARAMETER CALIBRATION FOR AKADAMA SOIL

The parameters of the proposed model are categorized into stress-strain relationship parameters ($\lambda, \Gamma, M, \nu_e, \kappa, \omega$) and particle crushing parameters ($\xi, \sigma_r, \chi, k_\eta$). By conducting several triaxial compression tests until reaching a critical state condition. Plotting the result in the specific volume, v versus the logarithm of mean effective stress, p' can be utilized to determine the critical state line (CSL). From this CSL we can determine: λ from the slope of CSL and Γ from the specific volume on CSL under atmospheric pressure. The slope of the critical state line in the q-p' plane, M and Poisson's ratio, ν_e can also be calibrated using the triaxial compression tests. κ can be derived from the slope of the swelling part by conducting a loading-unloading isotropic consolidation test. Parameter ω can be calibrated afterward to fit simulation results to experimental data at different densities. ξ defines the volumetric distance between SBSs of I_G = 0 and 1.

4.1.1 Experiment data of Akadama soil

In order to discuss the performance of the proposed model considering particle crushing, the model will be validated with the triaxial tests of a crushable volcanic soil, Akadama soil. The experimental data used in this research is derived from the triaxial tests conducted by OYO Corporation. It is volcanic soil derived from a loamy layer of soil in Ibaraki, Japan. The microscopic view of the soil particle is shown in Figure 4-1.

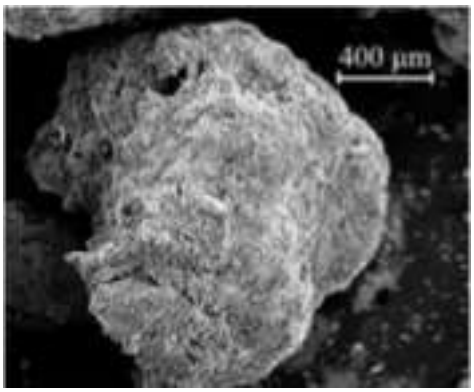

Figure 4-1 Microscopic view of Akadama soil

From the microscopic view of the soil particle, it is shown that the material is porous soil and vulnerable to crushing. The sample is initially uniformly graded with a diameter of less than 9.5 mm. The soil has solid density, ρ_s, 2.742 g/cm^3. The minimum and maximum dry densities, ρ_{dmin} and ρ_{dmax} are 0.600 and 0.696 g/cm, respectively. Cylindrical specimens under a fully saturated condition with a diameter of 50 mm and a height of 100 mm were prepared. The initial dry density of the specimens is around 0.699 g/cm^3 (specific volume of 3.92) and the initial confining stress was 20 kPa.

The triaxial tests were performed to investigate the particle crushing affected under several different stress paths. The confining pressures are varied with the value of 98 kPa, 196 kPa, 340 kPa, and 588 kPa, respectively. An unloading path was applied in each case of the experiment to capture the swelling index, k, in the v-ln p' relationship, to depict the elastic relationship in the simulation. The shearing was performed after conducting isotropic compression until it reached 0.25 of axial strain.

A sieving test was performed after conducting each test to check the evolution of grading from initial, uniform grading. The measured particle size distribution after each test is illustrated in Figure 4-2. It is observed that an increase in effective stress levels leads to a higher degree of crushing. Shearing induces more particle breakage compared to an isotropic compression test. Additionally, when comparing tests conducted under the same confining pressure, the drained shearing test results

in more significant crushing compared to the undrained shearing test. The I_G of each experiment is calculated using Eq. (2-6). Limiting grading is defined by employing the theory of fractal grading by Tyler and Wheatcraft (1992).

$$\frac{M(r < R)}{M_T} = \left(\frac{R}{R_L}\right)^{3-D} \tag{4-1}$$

where $M(r < R)$ is the mass of the material less than the diameter R. M_T is the total mass and R_L is the maximum diameter of the soil specimens. Parameter D is the fractal dimension. For soil particles, the fractal dimension, D is determined to be $0 < D < 3$. By assigning $D = 2.55$, the limiting grading is defined as shown in Figure 4-2.

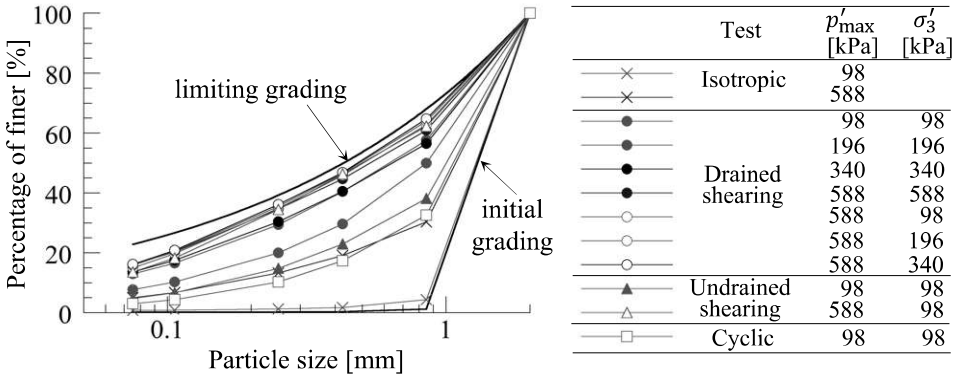

Figure 4-2 Particle size distribution before and after tests with the defined limiting grading

4.2 SIMULATION OF AKADAMA SOIL

The analysis has been carried out with several loading conditions based on the experiment data provided. The parameter set for Akadama soil is listed in Table 4-1 and Table 4-2.

Table 4-1 Constitutive parameters of Akadama soil for the proposed model

Parameter	Value	Description
λ	0.27	Compression index
Γ	3.13	Specific volume on CSL at atmospheric pressure, p_a

M	1.50	Critical stress ratio
ν_e	0.30	Poisson's ratio
κ	0.03	Swelling index
ω	2000	Effect of density
ξ	0.55	Volumetric distance between SBSs of I_G = 0 and 1

Table 4-2 Parameters for the evolution of grading due to particle crushing for Akadama soil

Parameter	Value	Description
σ_r	450	Crushing stress resistance [kPa]
χ	15	Rate of crushing
k_η	1.7	Effect of shearing on crushing

4.2.1 Isotropic consolidation tests

The comparison between the simulation and experiment of Akadama soil under isotropic compression can be seen in Figure 4-3. The soil is compressed until reaching mean effective stress of 98 kPa and 588 kPa. In both cases, the proposed model is able to predict the change in specific volume accurately. In addition, the final grading index I_G for isotropic compression to both stress states is predicted well through the proposed model.

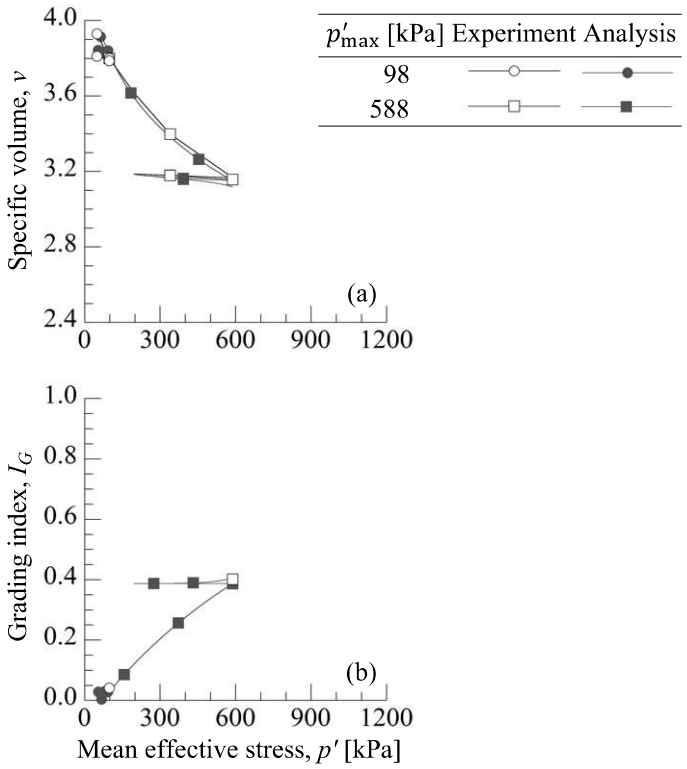

Figure 4-3 Comparison between experiment data and simulation results of Akadama soil under isotropic compression tests

4.2.2 Drained triaxial tests

The result of the drained triaxial test can be seen in Figure 4-4 and Figure 4-5. The results shown in Figure 4-4 are that the maximum mean effective stress applied before shearing is equal to the minor principal stress applied from the radial direction before shearing. Those are indicated by p'_{max} and σ'_3 respectively. The soil is compressed isotropically to 98, 196, 340, and 588 kPa then sheared under the same stress level. Based on the results, the model satisfactorily captured the behavior of crushable Akadama soil under drained triaxial tests. The volumetric behavior of the soil is predicted well through the simulation. The stress-strain relationship can also be simulated by the model. In Figure 4-5, all the soils were compressed until reaching 588 kPa. It was then unloaded to 98, 196, and 340 kPa and sheared. Under these loading paths, the model can also predict the experiments well.

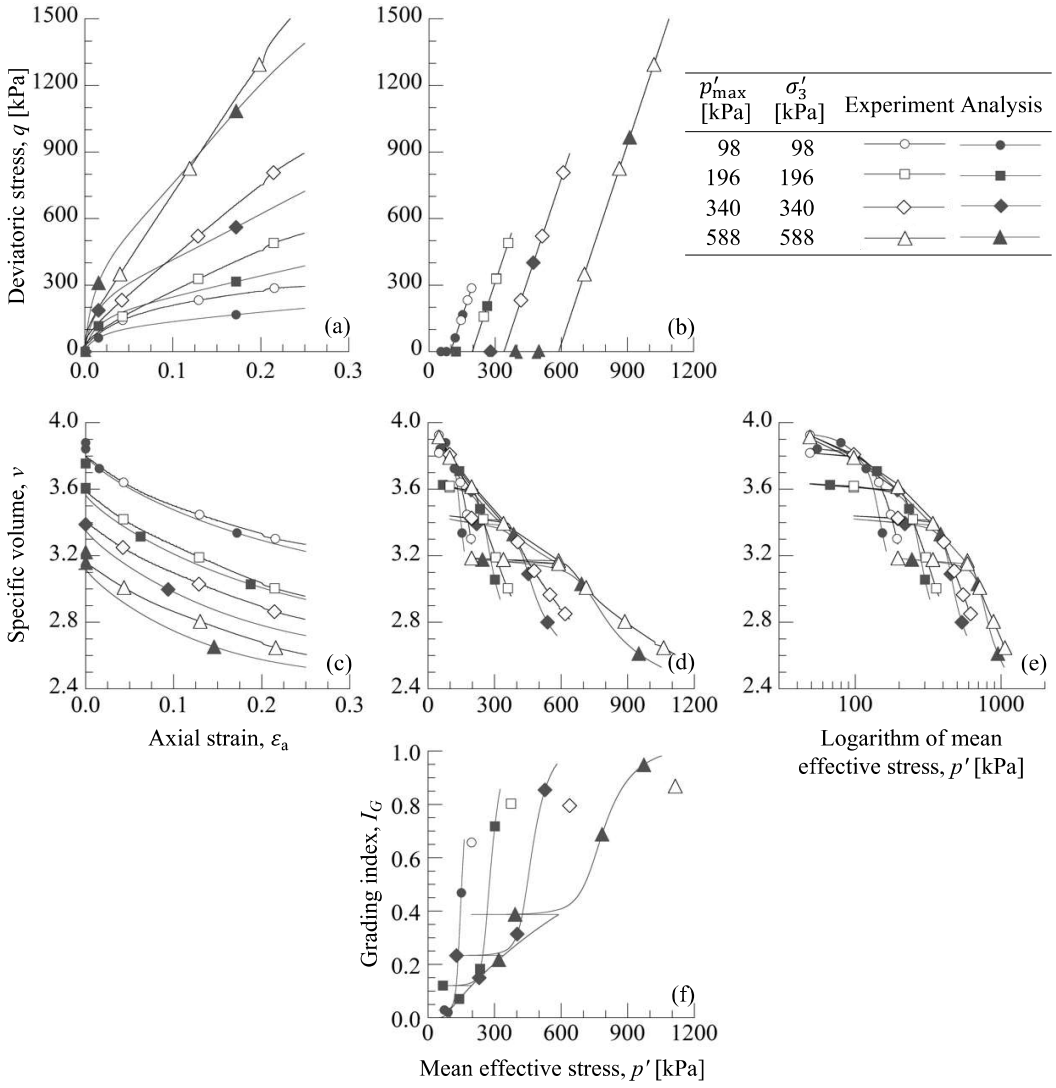

Figure 4-4 Comparison between experiment data and simulation results of Akadama soil under drained triaxial tests

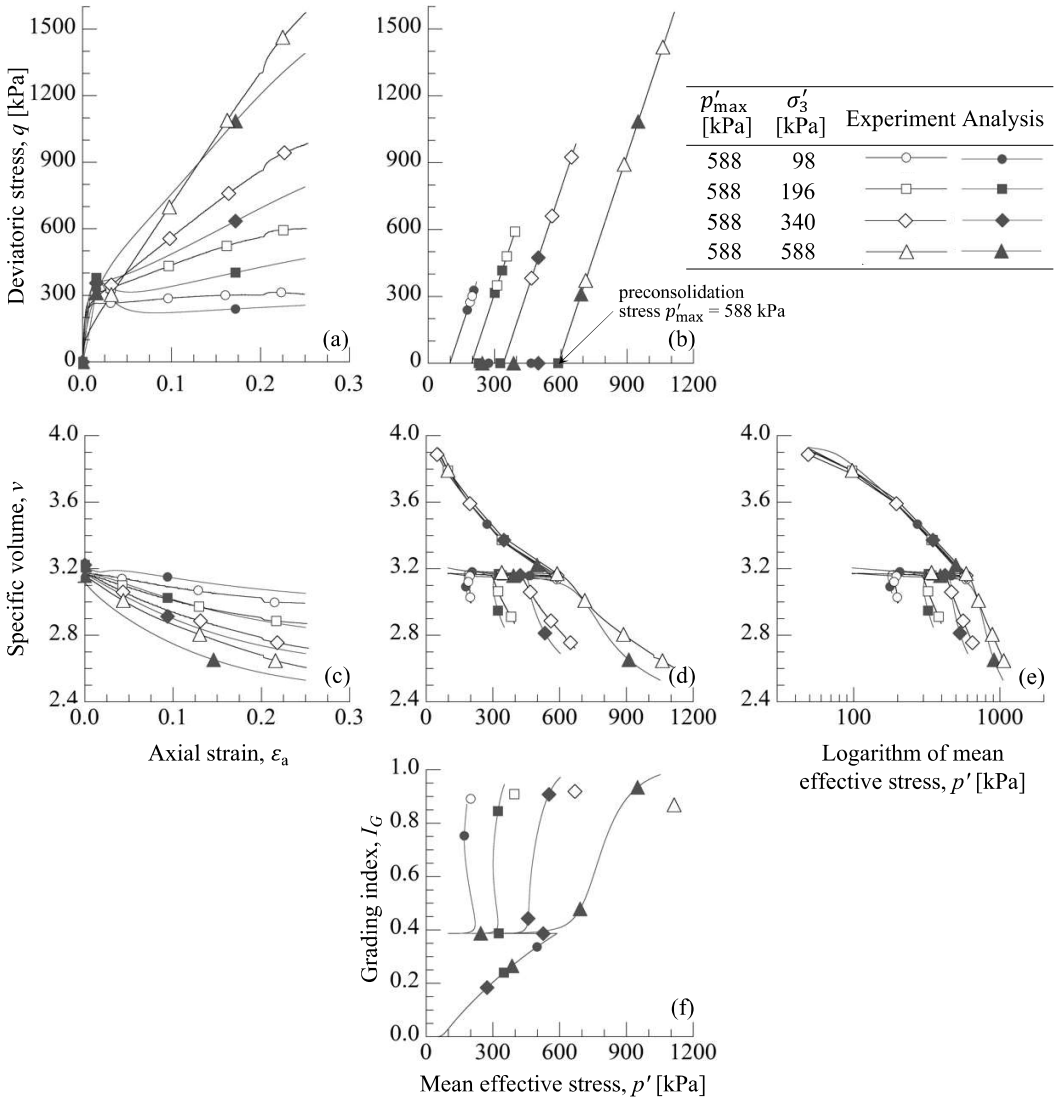

Figure 4-5 Comparison between experiment data and simulation results of Akadama soil under drained triaxial tests with unloading path

4.2.3 Undrained triaxial tests

Undrained triaxial tests were performed and simulated, as depicted in Figure 4-6. Two scenarios were examined, with both cases subjected to shearing at 98 kPa. However, the second case involved initially compressing the specimen to 588 kPa before unloading it to 98 kPa. Notably, the results reveal a substantial distinction

between the two scenarios. Nevertheless, the proposed model successfully predicts the behavior in both cases.

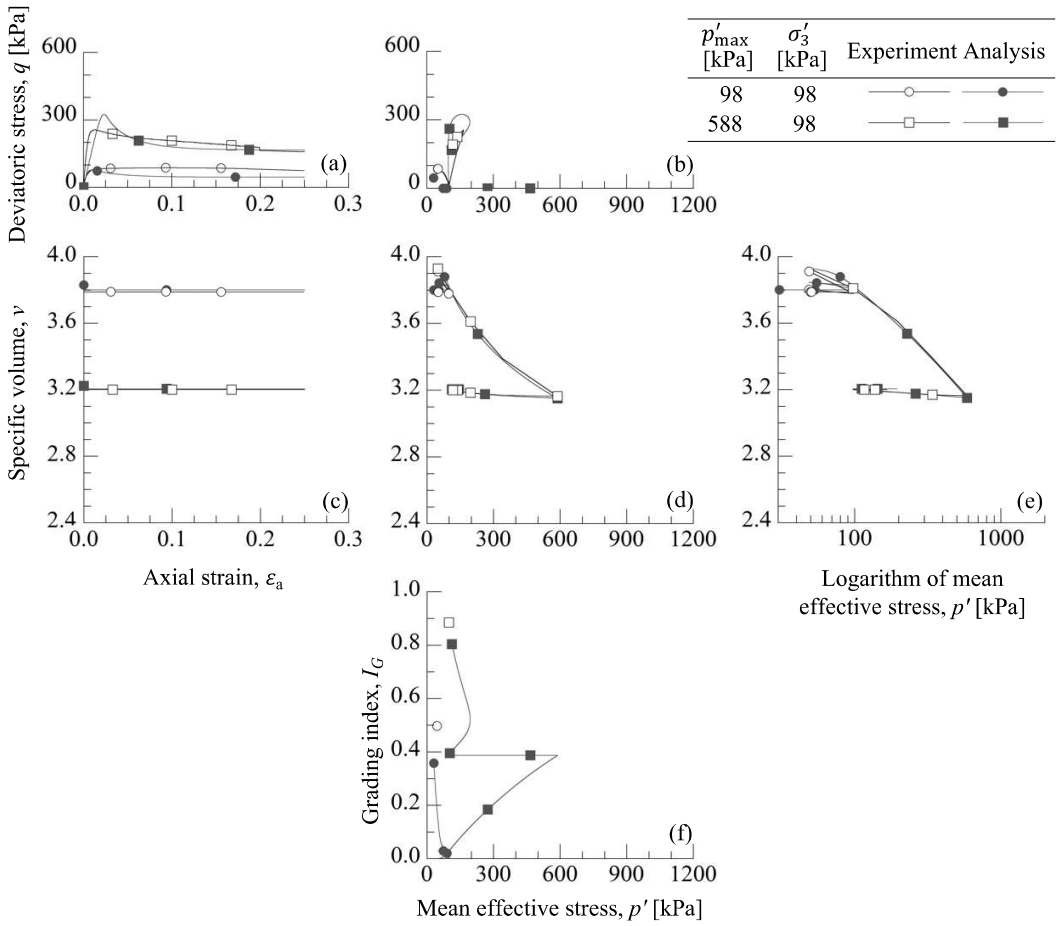

Figure 4-6 Comparison between experiment data and simulation results of Akadama soil under undrained triaxial tests

4.2.4 Undrained cyclic triaxial test

Figure 4-7 presents the outcome of undrained cyclic triaxial tests. After subjecting the soil to cyclic loading, it was subsequently sheared to a value of 0.25. The results indicate that even during cyclic loading, the stress state gradually reduces but this model is able to accommodate the gradual increase in grading, albeit at a slow rate. Within the maximum stress level, we were able to predict the progressive variation in grading. The difference in the stress path can be attributed to the specimen having an effective stress b-value of less than 1 or the specimen

being slightly unsaturated. As a consequence, when we apply increasing mean effective stress, p, the soil tends to be more compressed. Another contributing factor is that we do not consider the difference in strength in compression and extension sides. Nevertheless, the model remains capable of capturing significant grading changes as shearing progresses, particularly during plastic deformation. This enables accurate prediction of crushing phenomena. Consequently, in scenarios such as cyclic loading during earthquakes, where crushable soil is prone to exhibiting crushing and sliding surface liquefaction, this model proves capable of predicting the continuous variation in grading resulting from crushing.

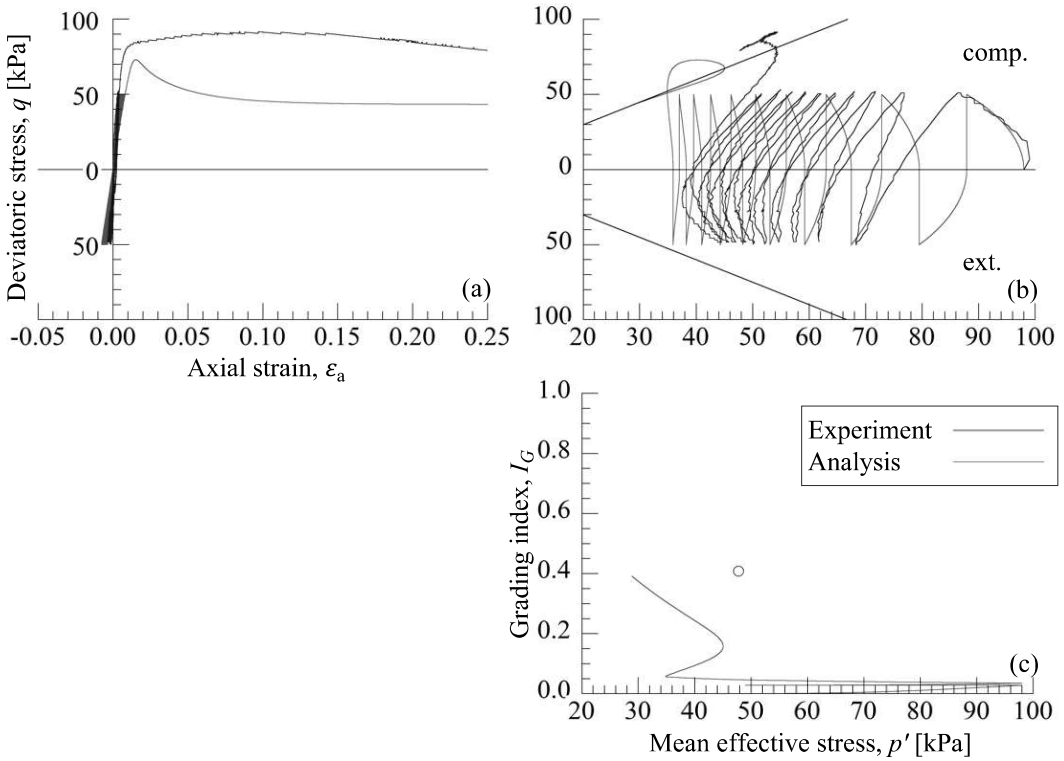

Figure 4-7 Comparison between experiment data and simulation results of Akadama soil under cyclic undrained triaxial tests

4.3 PARAMETRIC STUDY

4.3.1 Comparison to the existing model

To highlight the importance of the proposed model, we need to compare it with the former model. Using the same parameter, but with the existing model, the grading index after experiment can be seen in Figure 4-8. The result shows that the model can predict the grading index for the one compressed to 588 kPa. However, for small stress level and especially for the tests with unloading path, the grading index cannot be predicted well using the existing evolution law. Similar tendency is also found in the undrained test.

To understand the mechanism, we analyze the concept in each model. In Figure 4-9, we compare both simulations under drained triaxial tests without an unloading path (similar to Figure 4-4). In the proposed model, use the concept of I_G^{max} and I_G will always try to reach I_G^{max}. On the other hand, the former model by Kikumoto et al. (2010) uses a crushing surface, f_c to determine whether the crushing occurs or not. Crushing surface, f_c is calculated as follows.

$$f_c = p' \left[1 + \frac{1}{2}\left(\frac{\eta}{M}\right)^3\right] - p_c = 0 \tag{4-2}$$

p_c is the maximum stress level that the soil has experienced. Grading index, I_G is defined as:

$$I_G = 1 - \exp\left(-\frac{p_c - p_{ci}}{p_r}\right) \tag{4-3}$$

where p_{ci} is the stress level at which soil having unit grading starts to crush and p_r is a constant to control the resistance of soils against crushing. In the shearing condition, the combination of the shearing effect and stress level will control the crushing. In this former model, the stress level is used as the evolution law of I_G without considering the deformation. In the first case, although the frameworks are different, both of the models can work well to simulate crushing happening in the soil.

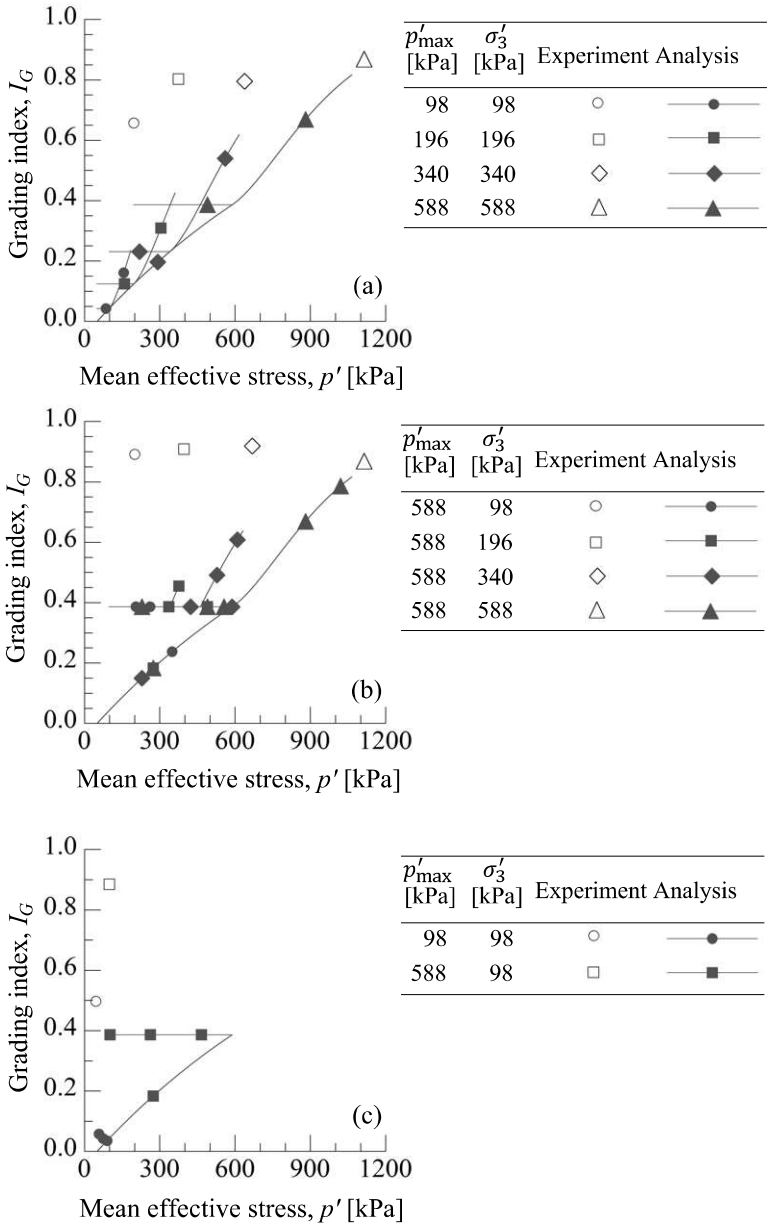

Figure 4-8 Simulation of Akadama soil using existing evolution law of crushing under (a) drained triaxial test; (b) drained triaxial test with unloading path; and (c) undrained triaxial test

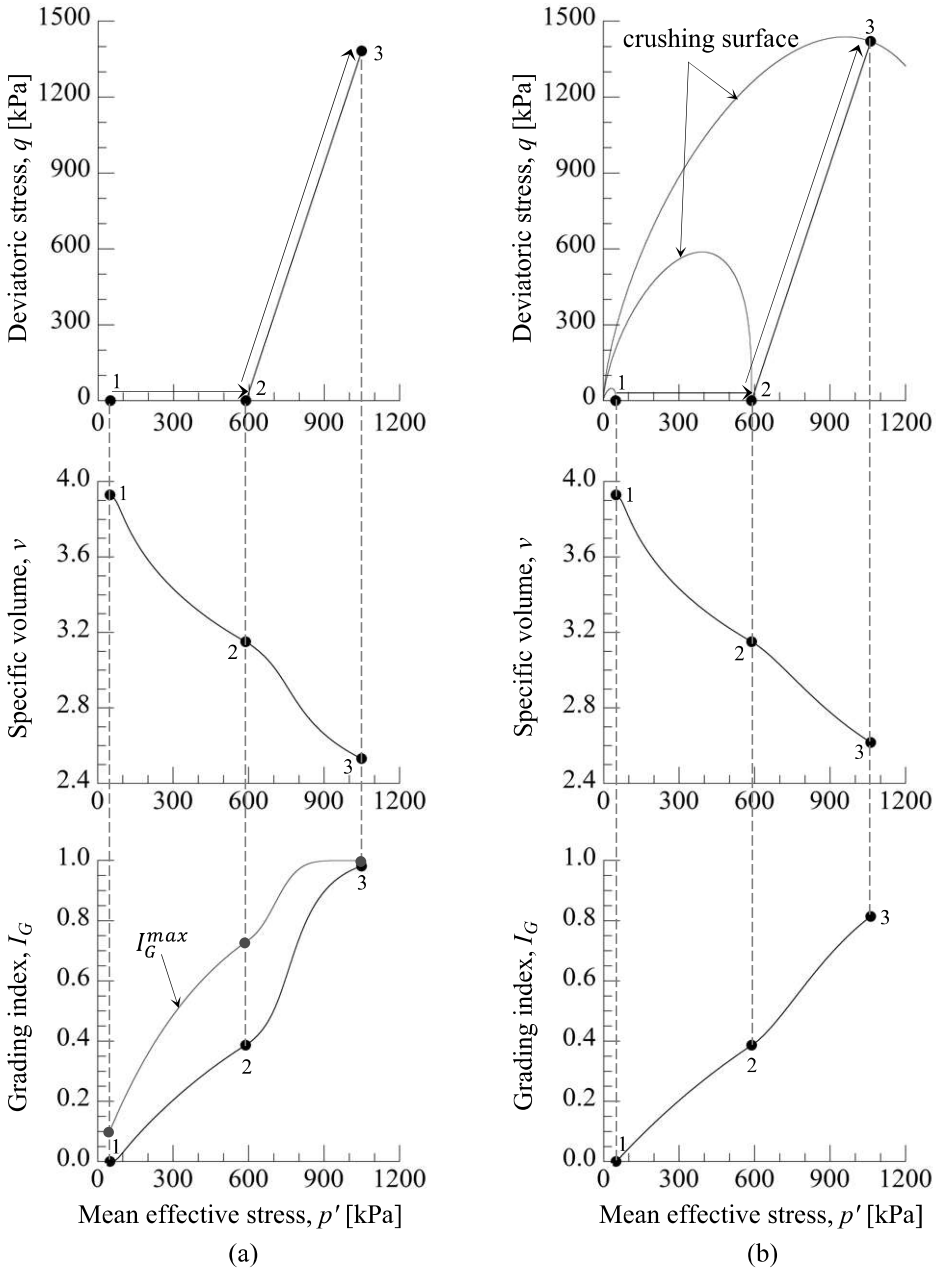

Figure 4-9 Comparison of the model concept of (a) the proposed model and (b) the former model under triaxial tests without unloading path

In the next case, we will see what will happen when we have an unloading path. This is similar to the simulation shown in Figure 4-5. where we compressed the soil until reaching 588 kPa before unloading it and shearing it. Using the proposed model, after unloading, we still have some gaps between I_G^{max} and current I_G. This

gap will be gradually filled and finally, our state is very close to the maximum I_G value and will eventually reach 1 if we shear it continuously (Figure 4-10 (a)).

However, using the former model, due to the unloading, the stress level was decreased and detached from the crushing surface. Inside the crushing surface, crushing will not occur. Therefore, at the beginning of shearing, we cannot identify any crushing. Crushing will again be recognized when the stress level reaches the largest crushing surface that has been created previously. As a result, the crushing will be underestimated (Figure 4-10 (b)).

The former model does not work well particularly when we have relatively small stress levels such as in cyclic loading and undrained triaxial tests. In the proposed model, we calculate grading change based on the stress level and the plastic deformation. I_G^{max} is defined by the current stress level. When we continue shearing or applying plastic deformation, the current grading state, I_G always has a distance to the maximum grading state, I_G^{max}, so grading will always try to increase to the ultimate state defined by the stress level. Using this concept, we are not limited to simulating any tests even when the stress levels are relatively low such as in cyclic loading.

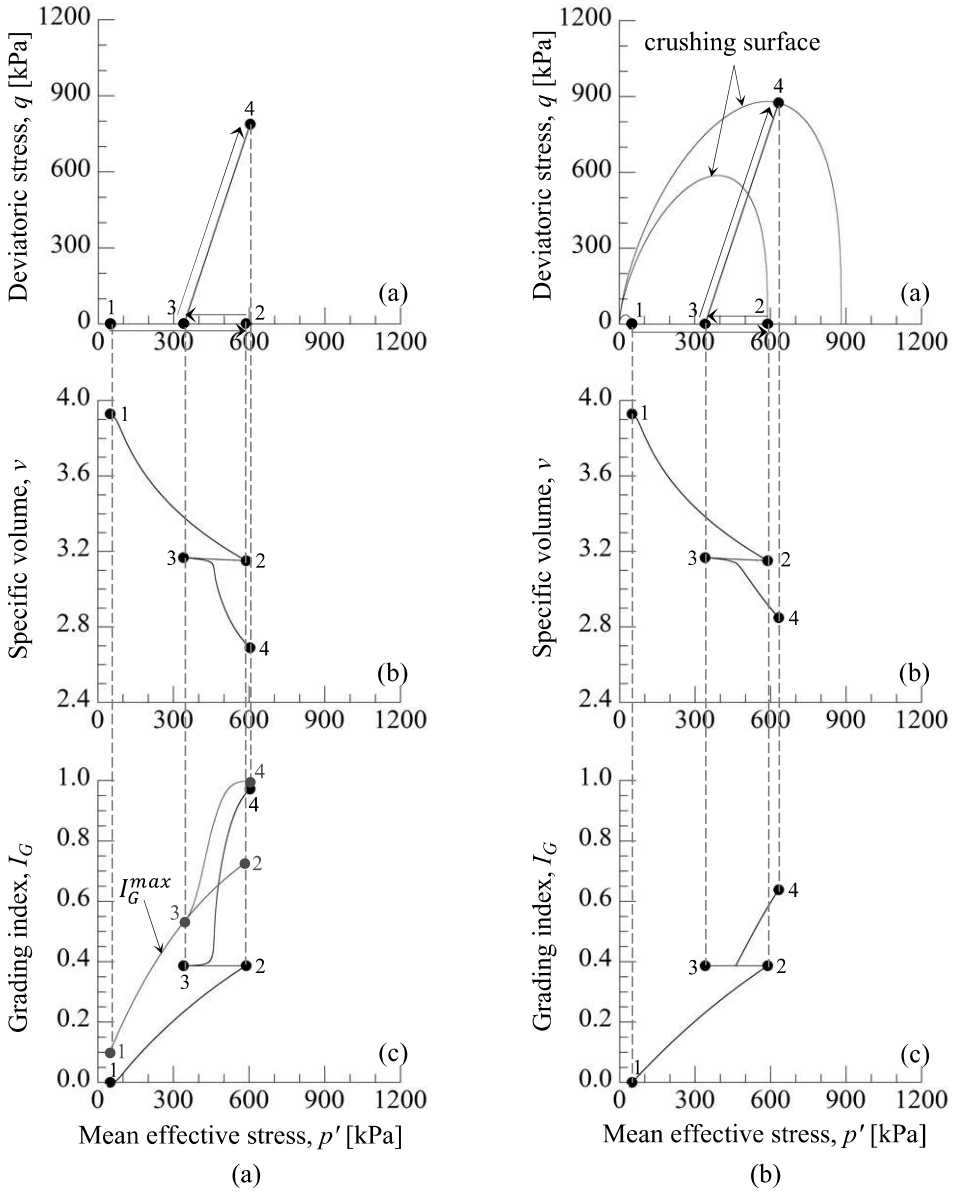

Figure 4-10 Comparison of the model concept of (a) the proposed model and (b) the former model under triaxial tests with unloading path

4.3.2 Crushing stress resistance (σ_r)

σ_r is a material constant defining crushing stress resistance. σ_r affects how the maximum grading index, I_G^{max}, increase to 1. Three different simulations using different σ_r value is shown in Figure 4-11. The higher the σ_r, its resistance to crushing is higher therefore the slower is the compression of the soil. However, eventually it will reach the same state when it achieved the critical state.

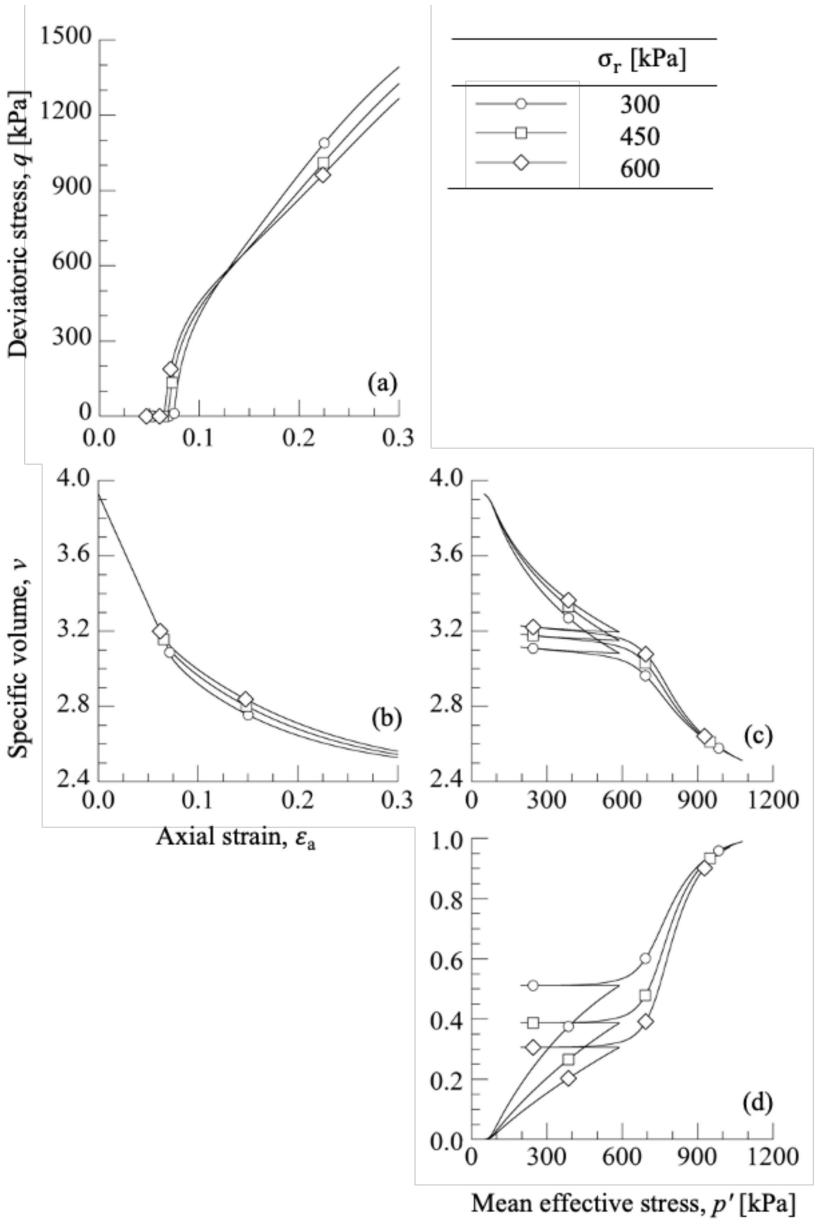

Figure 4-11 Effect of material parameter crushing stress resistance, σ_r on the model responses

4.3.3 Rate of crushing (χ)

The rate of crushing can be adjusted by the material parameter, χ. The effect of χ can be seen in Figure 4-12. A higher χ value makes the crushing faster and vice versa.

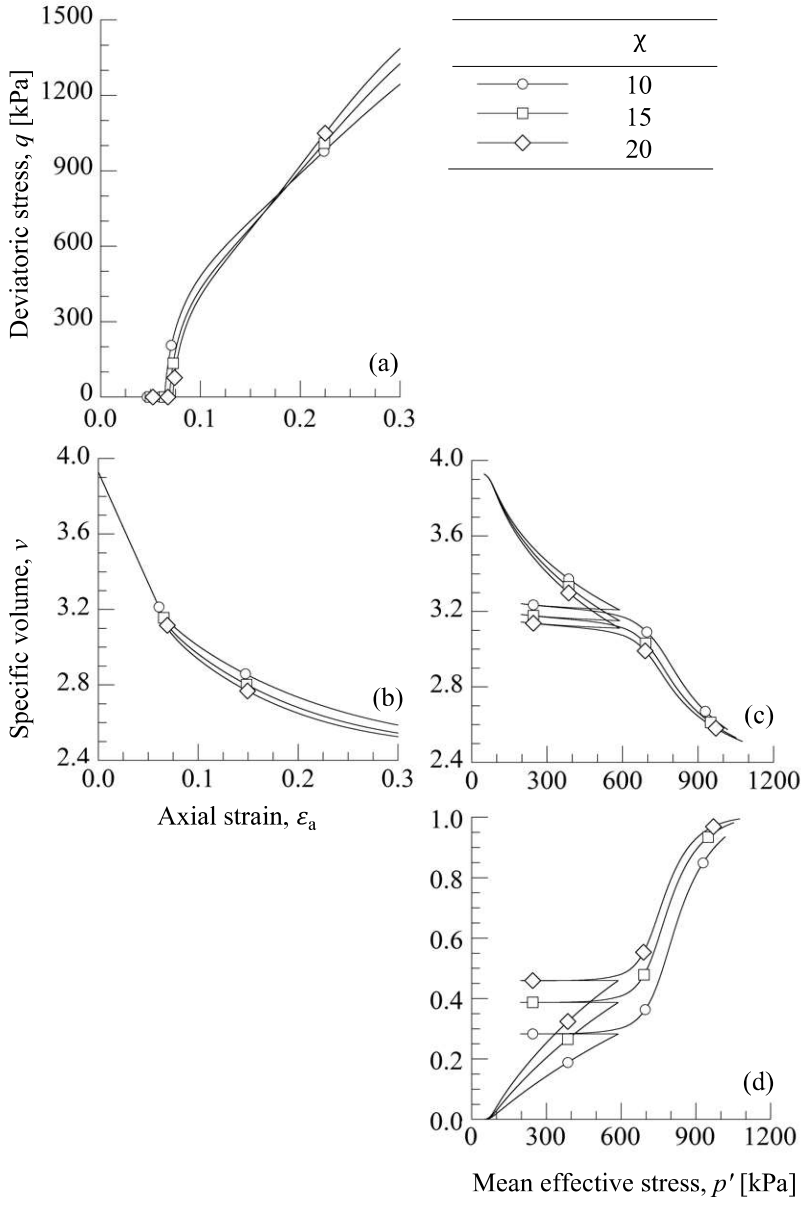

Figure 4-12 Effect of material parameter rate of crushing, χ on the model responses

4.3.4 Effect of shearing on crushing (k_η)

To control the effect of shearing on crushing, material parameter k_η is used. According to its definition, this parameter will only affect the shearing part of the simulation (Figure 4-13).

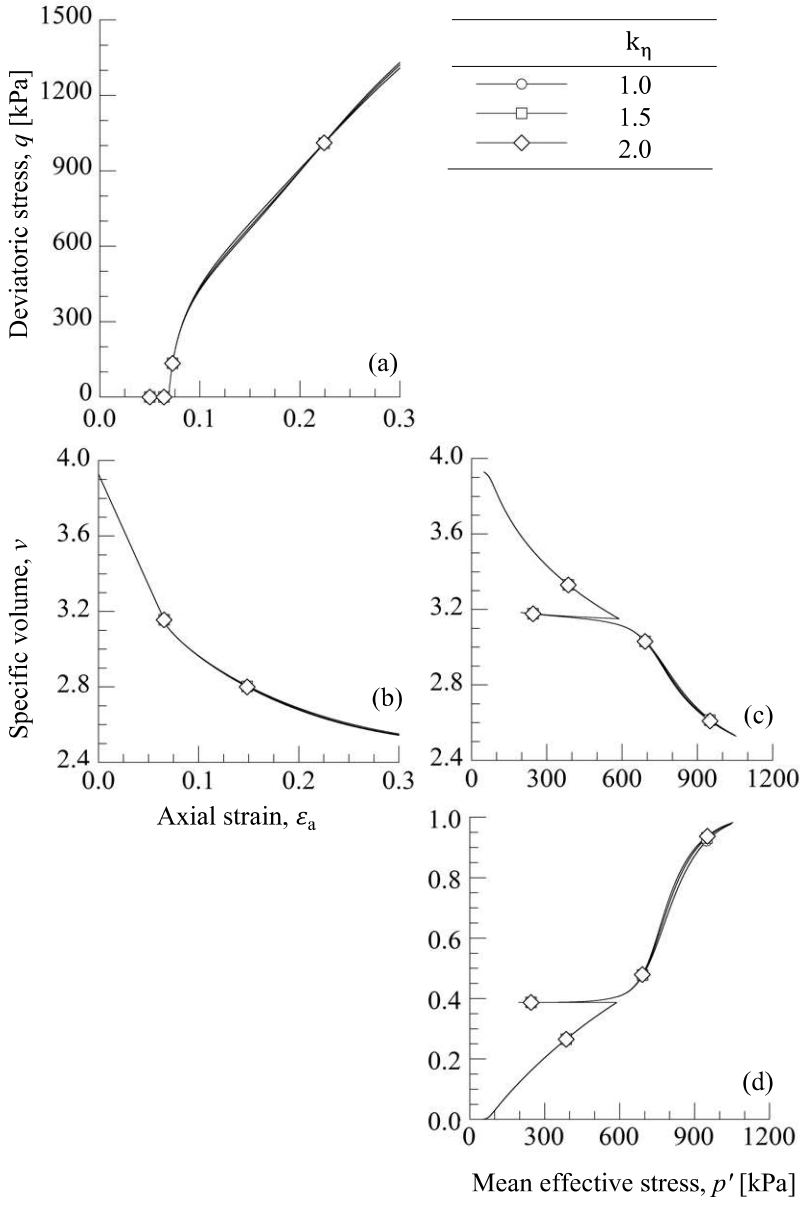

Figure 4-13 Effect of material parameter k_η on the model responses

4.3.5 Crushable and uncrushable

Analyzing the characteristics of soils that can be crushed and those that cannot be crushed is a complex task when conducted through experiments. Finding soil samples with identical mechanical properties but varying crushability is challenging. Nevertheless, this investigation can be accomplished through

simulation. In this model, uncrushable soils can be simulated by simply changing the crushing stress resistance, σ_r to a very large number so that the soil will not be crushed. The other parameters will be kept comparing two soils with the same mechanical properties but different crushing behavior.

The comparison of the behavior of crushable and uncrushable soils under drained tests is shown in Figure 4-14.

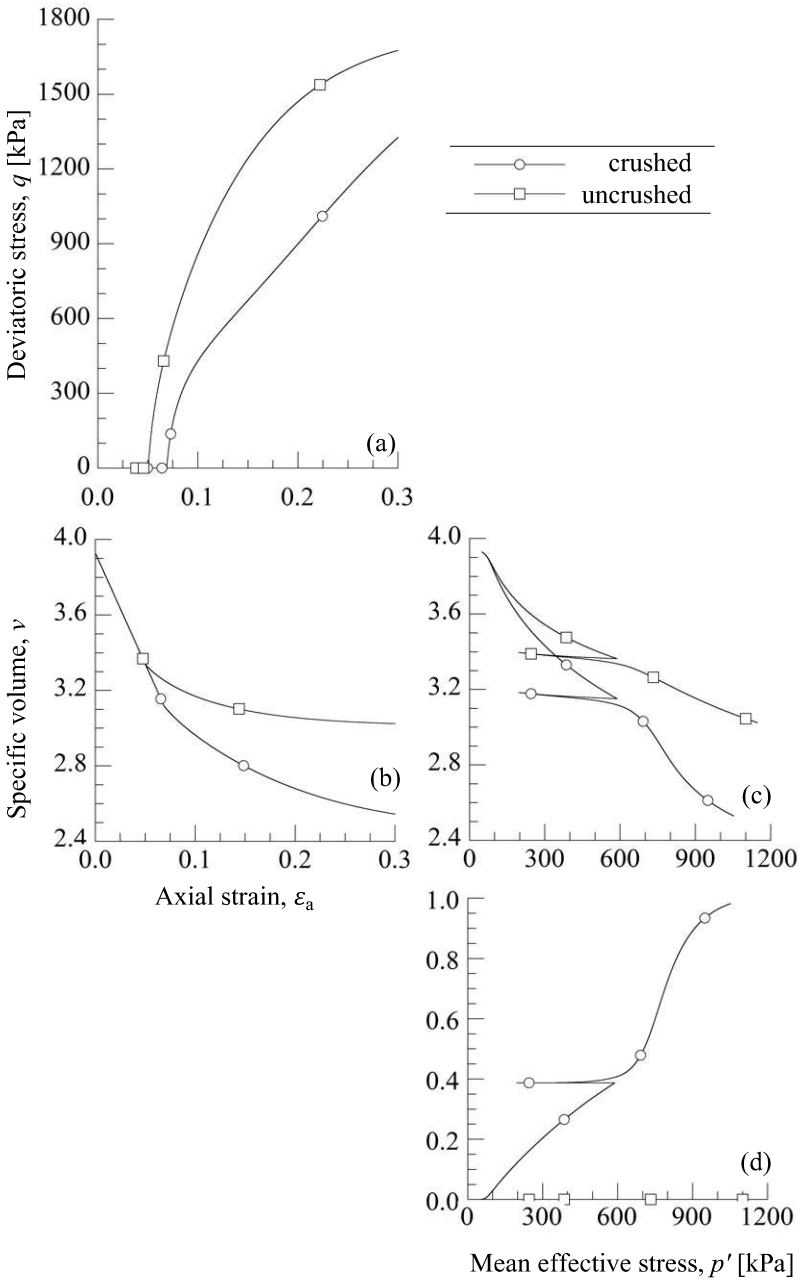

Figure 4-14 Comparison of crushed and uncrushable soil with the same parameter setting

CHAPTER 5
CONCLUDING REMARKS AND FUTURE RESEARCH

5.1 CONCLUSION

In this study, a critical state constitutive model for crushable soil with a generalized evolution law of grading has been proposed and validated. From the simulation result, we found that the proposed constitutive model could predict the behavior of the crushable soil well. The model can predict the behavior of crushable soil under the triaxial tests. More importantly, the model can be utilized to simulate the soil under small stress levels such as when doing cyclic undrained triaxial tests. A parametric study has also been conducted to understand the characteristics of the model.

5.2 FUTURE RESEARCH

Some recommendations for future research efforts can be focused on:

1) Consideration of anisotropy of soil to improve the result of cyclic loading simulation. For this, instead of applying isotropic hardening, implementing kinematic hardening into the model can be an option.
2) Application of the model to practical geotechnical problems to provide valuable insights into real-world performance.

REFERENCES

Been, K. and Jefferies, M. G. (1985). "A state parameter for sands." *Géotechnique*, *35*(2), 99-112.

Coop, M. R. and Lee I. K. (1993). "The behaviour of granular soils at elevated stresses." Predictive soil mechanics Edited by GT Houlsby and AN Schofield. Thomas Telford: London, UK, 186-199.

Coop, M. R., Sorensen, K. K., Bodas Freitas, T. and Georgoutsos, G. (2004). "Particle breakage during shearing of a carbonate sand." *Géotechnique*, *54*(3), 157-163.

Daouadji, A. and Hicher, P. Y. (2010). "An enhanced constitutive model for crushable granular materials." *International journal for numerical and analytical methods in geomechanics, 34*(6), 555-580.

Einav, I. (2007). "Breakage mechanics—Part I: Theory." *Journal of the Mechanics and Physics of Solids*, *55*(6), 1274-1297.

Einav, I. (2007). "Breakage mechanics—Part II: Modelling granular materials." *Journal of the Mechanics and Physics of Solids*, *55*(6), 1298-1320.

Gajo, A. and Wood, M. (1999). "Severn–Trent sand: a kinematic-hardening constitutive model: the q–p formulation." *Géotechnique*, *49*(5), 595-614.

Gale, D., Kuhn, H. W. and Tucker, A. W. (1951). "Linear programming and the theory of games." *Activity analysis of production and allocation*, *13*, 317-335.

Hardin, B. O. (1985). "Crushing of soil particles." *Journal of Geotechnical Engineering*, *111*(10), 1177-1192.

Hyodo, M., Hyde, A. F., Aramaki, N. and Nakata, Y. (2002). "Undrained monotonic and cyclic shear behaviour of sand under low and high confining stresses." *Soils and Foundations*, *42*(3), 63-76.

Kikumoto, M., Wood, D.M. and Russell, A. (2010). "Particle crushing and deformation behaviour." *Soils and Foundations*, *50*(4), 547-563.

Lade, P. V., Yamamuro, J. A. and Bopp, P. A. (1996). “Significance of particle crushing in granular materials.” *Journal of Geotechnical Engineering*, *122*(4), 309-316.

Lee, K. L. and Farhoomand, I. (1967). “Compressibility and crushing of granular soil in anisotropic triaxial compression.” *Canadian Geotechnical Journal*, *4*(1), 68-86.

Luzzani, L. and Coop, M.R. (2002). “On the relationship between particle breakage and the critical state of sands.” *Soils and foundations*, *42*(2), 71-82.

Marsal, R. J. (1967). “Large scale testing of rockfill materials.” *Journal of the Soil Mechanics and Foundations Division*, *93*(2), 27-43.

McDowell, G. R., Nakata, Y. and Hyodo, M. (2002). “On the plastic hardening of sand.” *Géotechnique*, *52*(5), 349-358.

Miura, N., Murata, H. and Yasufuku, N. (1984). “Stress-strain characteristics of sand in a particle-crushing region.” *Soils and Foundations*, *24*(1), 77-89.

Muir Wood, D. (2007). “The magic of sands—the 20th Bjerrum Lecture presented in Oslo, 25 November 2005.” *Canadian Geotechnical Journal*, *44*(11), 1329-1350.

Nakata, A. F. L., Hyde, M., Hyodo, H. and Murata. (1999). “A probabilistic approach to sand particle crushing in the triaxial test.” *Géotechnique*, *49*(5), 567-583.

Nguyen, V. P. and Kikumoto, M. (2018). “An elastoplastic model for soils exhibiting particle breakage.” In *Proceedings of the 4th Congrès International de Géotechnique-Ouvrages-Structures: CIGOS 2017, 26-27 October, Ho Chi Minh City, Vietnam 4* (pp. 644-655). Springer Singapore.

Oldecop, L. A. and Alonso, E. E. (2001). “A model for rockfill compressibility.” *Géotechnique, 51*(2), 127-139.

Pestana, J. M. and Whittle, A. J. (1995). “Compression model for cohesionless soils.” *Géotechnique, 45*(4), 611-631.

Russell, A. R. and Khalili, N. (2002). “Drained cavity expansion in sands exhibiting particle crushing.” *International Journal for Numerical and Analytical Methods in Geomechanics*, *26*(4), 323-340.

Senders, M., Banimahd, M., Zhang, T. and Lane, A. (2013). “Piled foundations on the North West Shelf.” *Australian Geomechanics 48*(4), 149-160.

Tyler, S. W. and Wheatcraft, S. W. (1992). “Fractal scaling of soil particle-size distributions: Analysis and limitations.” *Soil Science Society of America Journal*, *56*(2), 362-369.

Wang, F. W., Sassa, K., and Wang, G. (2002). “Mechanism of a long-runout landslide triggered by the August 1998 heavy rainfall in Fukushima Prefecture, Japan.” *Engineering Geology*, *63*(1-2), 169-185.

Wu, Y., Yamamoto, H., Cui, J. and Cheng, H. (2020). “Influence of load mode on particle crushing characteristics of silica sand at high stresses.” *International Journal of Geomechanics, 20*(3), 04019194.

Yasufuku, N., Murata, H., and Hyodo, M. (1991). “Yield characteristics of anisotropically consolidated sand under low and high stresses.” *Soils and Foundations*, *31*(1), 95-109.

Zhang, S., Li, R., Wang, F., and Iio, A. (2019). “Characteristics of landslides triggered by the 2018 Hokkaido Eastern Iburi earthquake, Northern Japan.” *Landslides, 16*, 1691-1708.

RESEARCH PUBLICATIONS

Florince and Kikumoto, M. (2023). “Modification of evolution law of grading for crushable soil.” In *The 34th KKHTCNN Symposium on Civil Engineering. KKHTCNN*. Pattaya, Thailand.